Journal of Earthquake Engineering

ISSN: 1363-2469 (Print) 1559-808X (Online) Journal homepage: www.tandfonline.com/journals/ueqe20

Source-Based Stochastic Response Analyses of Structures Using a Seismological Fourier Amplitude Spectral Model

Dengke Jiu , Haizhong Zhang & Yan-Gang Zhao

To cite this article: Dengke Jiu , Haizhong Zhang & Yan-Gang Zhao (05 Jan 2026): Source-Based Stochastic Response Analyses of Structures Using a Seismological Fourier Amplitude Spectral Model, Journal of Earthquake Engineering, DOI: 10.1080/13632469.2025.2607476

To link to this article: https://doi.org/10.1080/13632469.2025.2607476

Published online: 05 Jan 2026.

JOURNAL OF EARTHQUAKE ENGINEERING
https://doi.org/10.1080/13632469.2025.2607476

Taylor & Francis
Taylor & Francis Group

Source-Based Stochastic Response Analyses of Structures Using a Seismological Fourier Amplitude Spectral Model

Dengke Jiu[a,b], Haizhong Zhang[c], and Yan-Gang Zhao[a,b]

[a]College of Architecture and Civil Engineering, Beijing University of Technology, Beijing, China; [b]Key Laboratory of Urban Security and Disaster Engineering of Ministry of Education, Beijing University of Technology, Beijing, China; [c]Eco-Science Course, Faculty of Agriculture, Yamagata University, Yamagata, Japan

ABSTRACT

Most existing power spectral models used in structural stochastic response analyses only account for site effects through parameters such as fundamental period and damping ratio. However, these site-based models lack an explicit consideration of seismic source and path characteristics, which are inherently critical factors. With the accumulation of knowledge and advancements in seismic exploration technologies in recent decades, detailed seismic source information has become increasingly accessible, making it now both desirable and feasible to conduct stochastic response analyses that integrate not only site conditions but also source and path effects. Therefore, this study proposes an end-to-end analytical framework that simultaneously accounts for source, path, and site effects to efficiently compute the structural stochastic responses, thereby achieving direct prediction from specific seismic source conditions to structural responses. The proposed framework employs a source-based Fourier amplitude spectrum (FAS) model coupled with a ground motion duration model to represent the entire seismic wave propagation process, which has been thoroughly investigated and validated using real seismic records. The FAS parameters can be adjusted to simulate specific seismic sources of interest in earthquake engineering. Then, analytical formulations are derived for the stochastic response analyses of widely used multiple-degree-of-freedom structural systems in the frequency domain, which also supports time-domain stochastic response analysis by converting FAS into time series. Finally, the proposed method is applied to a series of numerical examples for reliability analysis, and the results are validated against time-domain analyses, demonstrating the applicability and accuracy of the method under varying seismic source conditions.

ARTICLE HISTORY
Received 15 July 2025
Accepted 15 December 2025

KEYWORDS
Structural stochastic response analysis; site-based power spectral models; seismic source; path characteristics; source-based Fourier amplitude spectral model

1. Introduction

As one of the essential tools for characterizing the seismic ground motions, power spectral models are commonly employed in stochastic structural response analysis (J. Li and Li 1998; Tootkaboni and Graham-Brady 2010; H. Zhang, Xiang, et al. 2023). The models currently employed here can generally be divided into two categories: one category is the traditional power spectral models (Liu, Liu, and Peng 2016; Ma et al. 2011; Peng, Mei, and Li 2014; Xu and Feng 2018; Zhao, Huang, and Hu 2020), such as Kanai-Tajimi model (Kanai 1962; Tajimi 1960), Clough-Penzien model (Clough and Penzien 1975), Hu model (Y. X. Hu and Zhou 1962), Ou model (Ou, Niu, and Du 1991), Li model (H. Li and Chen 2014) among others. While the other is the power spectral density function derived from the response spectrum (H. Hu et al. 2023) specified in seismic codes (GB50011-2010 Code). Comparing

CONTACT Haizhong Zhang zhang@tds1.tr.yamagata-u.ac.jp Eco-Science Course, Faculty of Agriculture, Yamagata University, 1-23, Wakaba-Machi, Tsuruoka-Shi, Yamagata 997-8555, Japan

these two categories, the traditional power spectral models demonstrate the better widespread applications, primarily due to the capability to effectively represent the ground motion resonance property induced by site conditions (Kanai 1962; Tajimi 1960). These models account for site effects by incorporating two key parameters, the site's fundamental period and damping ratio, which are calibrated through regression analysis of actual seismic records from different site classifications. The abovementioned models fundamentally qualify as site-based models, as they characterize ground motions at a specific site by matching recorded seismic data with known site parameters (Rezaeian and Der Kiureghian 2008).

Despite the widespread application of above site-based power spectral models, they do not explicitly incorporate seismic source and path characteristics, which are inherently critical factors influencing ground motion and structural stochastic response (Abdelnaby and Elnashai 2014; Calvi and Andreotti 2022; Estêvão and Carvalho 2015; Khansefid and Bakhshi 2022; Luo and Peng 2024; Naserieh et al. 2022). To characterize the effects of these factors, D. Wang and Li (2011) proposed a complete stochastic model of ground motions by combining the spectral transfer function with physical models of the seismic source, path, and site conditions. In this model, the seismic source is represented by the Brune dislocation model (Brune 1970), the path is described by the friction attenuation and the associated relationship between wavenumber and frequency, with the local site represented by a single-degree-of-freedom (SDOF) system. Then, this model was improved by providing the distribution of source parameters, including magnitude, distance, and site category, according to 7778 actual seismic records (Ding, Peng, and Li 2018). Based on this physical stochastic model, Ding, Xu, and Miao. (2022) generated numerous time series with varying magnitudes, distances, and site-specific shear-wave velocities and conducted stochastic response analysis of a five-layer reinforced concrete frame structure. The results demonstrate that as magnitude and distance increase, the long-period components of the ground motions are amplified, making the structure carry a higher risk of failure than the results from response spectrum method. Similarly, C. Zhang et al. (2022) employed the probability density evolution method to discretize the source and path parameters and generated numerous corresponding time series. Based on these excitations, stochastic response analysis of the aqueduct structure was conducted, which demonstrated the substantial influences of source and path factors on structural stochastic response results.

All these studies have proved that not only site conditions, but also the seismic source and path characteristics are inherently crucial factors in stochastic response analyses of structures, which cannot be neglected. Although the physical models mentioned above incorporate these factors, they still lack sufficient validation using real seismic records in the field of seismology.

With the accumulation of knowledge and advancements in seismic exploration technologies in recent decades, detailed seismic source information has become increasingly accessible. Japan-Seismic Hazard Information Station can provide the major fault zones distribution, detailed seismic source information (Morikawa et al. 2024). For more regions, Global Active Faults Database contains detailed information on over 11,000 seismic sources across Europe, Asia, America, and other regions. This database includes the parameters of source and fault location, length, strike, dip orientation, surface area et al. (Styron and Pagani 2020). This increasingly comprehensive source of information has made it both desirable and feasible to conduct stochastic response analyses that integrate not only site conditions but also source and path effects.

Therefore, this study proposes an end-to-end analytical framework for stochastic structural response analysis, which directly simulates the entire process from specific seismic source conditions to structural responses in the frequency domain, achieving a physical coupling between seismic motion modeling and structural response analysis. In terms of physical modeling, the proposed framework employs a source-based Fourier amplitude spectrum (FAS) model combined with a ground motion duration model (Boore and Thompson 2012, 2014) to capture the complete seismic wave propagation process from seismic source to ground surface. This FAS model has been thoroughly investigated and verified using real seismic records (Atkinson and Boore 2014; Boore 2003) and has been extensively used by numerous studies (Kottke and Rathje 2013; Rathje and Ozbey 2006;

X. Wang and Rathje 2016; H. Zhang and Zhao 2022). By decomposing the FAS model into source, propagation path, and site condition components, the model can be flexibly adjusted according to known seismic source and path parameters (Boore 1983, 2003), thereby enhancing its physical interpretability and applicability. At the theoretical level, analytical formulations are derived for the frequency-domain stochastic response of multi-degree-of-freedom (MDOF) structural systems, which can also be extended to time-domain analysis through a corresponding transformation between the FAS and time series. This unified computational framework preserves both the efficiency in frequency domain and accuracy in time series domain, providing a more comprehensive and reliable tool for stochastic structural response analysis.

The rest of this paper is organized as follows. Section 2 introduces the source-based FAS model. Within the proposed framework, Section 3 derives the theoretical formulations for the stochastic response analyses of widely used MDOF structural systems in the frequency domain. To demonstrate the feasibility and effectiveness of the proposed framework, a series of numerical examples are presented in Section 4, with analyses conducted in both frequency and time domains. Finally, the conclusions are summarized in Section 5.

2. Fourier Amplitude Spectral Model

To describe the seismic ground motions for structural stochastic response analyses, this study applies a source-based FAS model that accounts for site conditions, as well as seismic source and path characteristics. A basic source-based model applies seismological principles to calculate the radiated FAS from a point source, considering source, path, and site effects (Meimandi-Parizi, Mahdavian, and Saffari 2023; R. Zhang, Zhao, and Zhang 2023). Therefore, this paper adopts the source-based FAS model (Boore 1983, 2003; Boore and Joyner 1997), which has been extensively validated by comparing with recorded seismic motions (Boore and Joyner 1997; Brune 1970, 1971; H. Zhang and Zhao 2022; H. Zhang, Zhao, et al. 2023). In this model, the ground acceleration FAS, $F(f)$, is defined as the product of source,path, and site terms:

$$F(f) = E(M_0,f)P(R,f)G(f) \tag{1}$$

where f refers to the frequency, R refers to the distance between the site and source, and M_0 refers to the seismic moment, which is mathematically connected to the moment magnitude M:

$$M_0 = 10^{1.5(M+10.7)} \tag{2}$$

The omega-squared source-based spectrum of Brune is widely employed to characterize the FAS of earthquakes (Brune 1970). This source-based spectrum is typically combined with the terms of path and site proposed by Boore (2003, 2005):

$$F(f) = [0.78\frac{\pi}{\rho\beta^3}M_0\frac{f^2}{1+(\frac{f}{f_c})^2}][Z(R)\exp(\frac{-\pi fR}{Q(f)\beta})][\exp(-\pi\kappa f)A(f)] \tag{3}$$

where ρ is the density and β is shear wave velocity of the crust. $Z(R)$ represents the geometrical spreading function, $Q(f)$ indicates the seismic anelastic attenuation, $A(f)$ refers to the site amplification. f_c is the corner frequency, indicating the lower value before the FAS begins to decay:

$$f_c = 4.9\times10^6\beta\left(\frac{\Delta\sigma}{M_0}\right)^{\frac{1}{3}} \tag{4}$$

where, $\Delta\sigma$ is stress drop.

To account for the fault rupture characteristics that are particularly significant in large-magnitude earthquakes, this study adopts the stochastic finite-fault modelling approach. In this model, a large fault is subdivided into multiple subfaults (Beresnev and Atkinson 1998), and the ground motions

generated by each subfault are computed using the point-source method and then superimposed at the observation point to obtain the overall ground motion. In practical applications, it is more convenient to capture the essential features of finite-fault ground motions within a single point-source simulation framework by introducing an appropriate equivalent point-source distance R_{PS}. On this basis, Boore (2009) proposed an effective point-source distance R_{EFF} to modify the source-to-site distance R. However, the limitation of R_{EFF} is that it depends on a specific source and receiver geometry. To address this issue, Boore and Thompson (2015) proposed a more general formulation of R_{PS}, which is expressed as

$$R_{PS} = \sqrt{R_{RUP}{}^2 + h^2} \tag{5}$$

where R_{PS} is the rupture distance, and h is a finite-fault factor expressed as

$$\log(h(M)) = \begin{cases} a_1 + b_1(\mathrm{M} - M_{t1}), \mathrm{M} \le M_{t1} \\ e_0 + e_1(\mathrm{M} - M_{t1}) + e_2(M - M_{t1})^2 + e_3(M - M_{t1})^3, \; M_{t1} \le \mathrm{M} \le M_{t2} \\ a_2 + b_2(\mathrm{M} - M_{t2}), \mathrm{M} \ge M_{t2} \end{cases} \tag{6}$$

In Equation 6, a_1, a_2, b_1, b_2, $e_0 - e_3$, M_{t1} and M_{t2} are coefficients that have been given by Boore and Thompson (2015).

The way the FAS varies with magnitude and distance also depends on the seismological parameters, which can be determined based on earthquake records from the target region. In this study, typical seismological parameter values used in Equation 3 and (Equation 4) are adopted from Boore and Thompson (2015) and given in Table 1.

Despite the source-based FAS model, a ground motion duration model is also needed as the inputs for stochastic response analyses of structures. The ground motion duration, D_{gm}, used in this study is a sum of the source duration, D_s, and what is called the path duration, D_p, which represents the elongation of motion due to wave propagation and scattering effects (Boore and Thompson 2015). In detail, the source duration D_s is given by $1/f_c$, in which the corner frequency f_c is given by the single-corner frequency model. And the path duration D_p suggested for Stable Continental Regions (SCRs) is unitized in this study and given in Table 2 (Boore and Thompson 2015).

It should be noted that although this source-based FAS model represents the primary effects of the seismic source, path, and site conditions in a simplified manner, it does not fully capture complex earthquake phenomena such as near-field effects and source directivity. This limitation can be overcome by incorporating more advanced FAS models that explicitly consider these effects within the proposed framework. As the present study mainly aims to establish a practical framework that

Table 1. Parameters used for the FAS model.

Model parameter	Setting
σ (bar)	400
κ (s)	0.006
ρ (g/cm^3)	2.8
β (km/s)	3.7
$A(f)$	Boore (2015)
$Z(R)$	Atkinson and Boore (1995, 2014)
$Q(f)$	Atkinson and Boore (1995, 2014)

Table 2. The path duration model for SCRs.

Parameter	Value							
R_{RUP} (km)	0	15	35	50	125	200	392	600
D_p (s)	0	2.6	17.5	25.1	25.1	28.5	46	69.1

simultaneously accounts for source, path, and site effects to efficiently compute structural stochastic responses, the integration of advanced FAS models will be pursued in future work.

3. Application of the FAS Model for Structural Stochastic Response Analyses

The crucial aspect of structural stochastic response analyses is the calculation of the failure probability of the system (Filiatrault et al. 2018; O'Reilly and Sullivan 2017). In practical applications, the failure probabilities of widely used MDOF structural systems are commonly assessed using the criterion of maximum inter-layer relative displacement responses (Song and Li 2025; Welch, Sullivan, and Calvi 2014; Xu et al. 2022). Therefore, the failure probability of an MDOF system, P_s, can be expressed as follows:

$$P_s = 1 - \prod_{i=1}^{n} P(\Delta x_{i,max} < x_{lim}) \tag{7}$$

where x_{lim} is the inter-layer relative displacement threshold, and $\Delta x_{i,max}$ is the maximum relative displacement response of the i-th inter-layer.

To compute the maximum inter-layer relative displacement response $\Delta x_{i,max}$, random vibration theory (RVT) can be applied (Hanks and McGuire 1981):

$$\Delta x_{i,max} = pf \times Dis_{rms} \tag{8}$$

where pf is the peak factor; Dis_{rms} is the root mean squared (RMS) value of the structural inter-layer relative displacement responses.

In Equation 8, the peak factor pf has been defined as the ratio of the maximum response to the RMS value by previous research, and numerous peak-factor models have been proposed (Cartwright and Longuet-Higgins 1956; Vanmarcke 1975). X. Wang and Rathje (2016) found that among the models evaluated, the Vanmarcke model (Vanmarcke 1975) provides the most accurate estimation of the peak factor. The cumulative distribution function (CDF), P, of pf, as formulated by Vanmarcke (1975), is expressed as

$$P(pf < r) = \left[1 - \exp\left(-\frac{r^2}{2}\right)\right] \exp\left\{-2f_z \exp\left(-\frac{r^2}{2}\right) D_{gm} \frac{\left[1 - \exp\left(-\sqrt{\frac{\pi}{2}}\delta^{1.2} r\right)\right]}{1 - \exp\left(\frac{r^2}{2}\right)}\right\} \tag{9}$$

where f_z is the rate of zero crossing, δ is the bandwidth factor.

On the other hand, the RMS value, Dis_{rms}, in Equation 8 can be estimated from the power spectrum of structural inter-layer relative displacement response $G_{\Delta out}(\omega)$:

$$Dis_{rms} = \sqrt{\frac{1}{\pi}\int_0^{\infty} G_{\Delta out}(\omega) d\omega} \tag{10}$$

Therefore, before analyzing the maximum inter-layer relative displacement responses, $G_{\Delta out}(\omega)$ should be estimated from the ground motion FAS and duration. Consider an MDOF system with verified mass, stiffness, and damping for each layer. The equation of motion under seismic excitation can be written as

$$[M]\{\ddot{x}(t)\} + [C]\{\dot{x}(t)\} + [K]\{x(t)\} = -\ddot{y}(t)[M]\{1\} \tag{11}$$

Here $\{x(t)\}$, $\{x(t)\}$, and $\{x\,(t)\}$ are response displacement, velocity, and acceleration response vector, respectively; $y\,(t)$ represents the ground acceleration. The matrixes $[M]$, $[C]$, and $[K]$ are the mass, damping, and stiffness, respectively.

By introducing the mode shape matrix, $[\phi]$, to represent the displacement vector $\{x(t)\}$, the modal equation of motion is obtained:

$$[M][\phi]\{q(t)\}+[C][\phi]\left\{\dot{q}(t)\right\}+[K][\phi]\{q(t)\}=-\ddot{y}(t)[M]\{1\} \tag{12}$$

Then, multiplying both sides of the Equation 12 by the transpose of the mode shape matrix, $[\phi]^T$, and exploiting the modal orthogonality, the coupled mass, damping, and stiffness matrices are diagonalized. This procedure decomposes the original MDOF system into a set of uncoupled SDOF systems, where each modal system is characterized by its corresponding modal mass, modal damping, and modal stiffness. The equation of motion for the j-th mode can be expressed as

$$\ddot{q}^{(j)}(t)+2\xi^{(j)}\omega^{(j)}\dot{q}^{(j)}(t)+\left(\omega^{(j)}\right)^2 q^{(j)}(t)=-\gamma^{(j)}\ddot{y}(t) \tag{13}$$

where $q^{(j)}(t)$ represents the j-th modal amplitude, $\xi^{(j)}$ and $\omega^{(j)}$ is the damping ratio and the undamped natural circular frequency of the j-th mode, and $\gamma^{(j)}$ is the mode participation factor.

Dividing Equation 13 by $\gamma^{(j)}$ yielding the modal amplitude under unit excitation, ${q_0}^{(j)}(t)$:

$$\ddot{q}_0{}^{(j)}(t)+2\xi^{(j)}\omega^{(j)}\dot{q}_0{}^{(j)}(t)+(\omega^{(j)})^2 q_0{}^{(j)}(t)=-\ddot{y}(t) \tag{14}$$

where $q^{(j)}(t)=\gamma^{(j)}{q_0}^{(j)}(t)$. Then, the displacement vector and inter-layer relative displacement are then obtained via modal superposition:

$$\{x(t)\}=\sum_{j=1}^{n}\left\{\gamma^{(j)}\phi^{(j)}\right\}q_0{}^{(j)}(t) \tag{15}$$

$$\{\Delta x(t)\}==\sum_{j=1}^{n}\left\{\gamma^{(j)}\Delta\phi_i{}^{(j)}\right\}q_0{}^{(j)}(t) \tag{16}$$

where $\Delta\phi_i{}^{(j)}=\phi_i{}^{(j)}-\phi_{i-1}{}^{(j)}$ represents the i-th inter-layer modal difference corresponding to the j-th vibration mode.

Then, the FAS of the response of structural i-th inter-layer relative displacement, $Fd_{i_{\Delta,out}}(\omega)$, can be obtained via time-frequency transformation:

$$\left\{Fd_{i\Delta,out}(\omega)\right\}=\sum_{j=1}^{n}\left\{\gamma^{(j)}\Delta\phi_i{}^{(j)}\right\}F_{out}{}^{(j)}(\omega)=\sum_{j=1}^{n}\left\{\gamma^{(j)}\Delta\phi_i{}^{(j)}\right\}H^{(j)}(\omega)F(\omega) \tag{17}$$

where $F(\omega)$ denotes the FAS model with respect to circular frequency ω, and $H^{(j)}(\omega)$ is the transfer function of the relative displacement corresponding to the j-th vibration mode.

On this basis, the response power spectrum of the i-th inter-layer relative displacement can be obtained:

$$G^{(i)}{}_{\Delta,out}(\omega)=\frac{\left(Fd^{(i)}{}_{\Delta,out}(\omega)\right)^2}{D_{rms}} \tag{18}$$

where D_{rms} denotes the duration of the structural response and can be calculated as

$$D_{rms}=D_{gm}\cdot\left(c_1+c_2\frac{1-\eta^{c_3}}{1+\eta^{c_3}}\right)\left[1+\frac{c_4}{2\pi\zeta}\left(\frac{\eta}{1+c_5\eta^{c_6}}\right)^{c_7}\right] \tag{19}$$

where $\eta=T_0/D_{gm}$, T_0 denotes the natural period of the structure. c_1-c_7 are coefficients that depend on the magnitude and distance, as noted in Boore and Thompson (2012). The c_e coefficients in Boore and Thompson (2014) were derived using the peak-factor model of Cartwright and Longuet-Higgins (1956). Boore and Thompson (2015) further updated the c_e coefficients using the peak-factor model of Vanmarcke (1975), which are adopted in this paper.

4. Numerical Examples

To demonstrate the feasibility and effectiveness of the proposed analytical framework, a series of numerical examples are presented in this section, with stochastic response analyses conducted in both the frequency and time series domains.

In the frequency domain, the CDF of the maximum inter-layer relative displacement responses is given by Equation 8 and (Equation 9), and the corresponding probability density function (PDF) is obtained by differentiating the CDF. Then, the structural failure probabilities were calculated using Equation 7 according to the threshold values specified in relevant structural codes.

In the time series domain, 100,000 time series were first generated to ensure the statistical stability of the calculation results by the FAS model using Stochastic Method Simulation (SMSIM) program proposed by Boore (1983, 2000, 2005). Second, the inter-layer relative displacement responses between each pair of adjacent layers for every individual time series were calculated, and the maximum response value among all inter-layers was identified. By statistically analyzing these maximum inter-layer relative displacement responses from 100,000 time series inputs, the respective PDF and CDF figures were presented. Then, based on the obtained maximum inter-layer relative displacement responses, the mean values were calculated and compared with the corresponding results derived from the frequency-domain analyses. Finally, the structural failure probabilities were evaluated in both the frequency and time series domains.

To primarily examine the effects of earthquake magnitude and distance, multiple magnitudes M of 5.0, 6.0, 7.0, and 8.0 and rupture distances R_{RUP} of 10 km, 50 km, 100 km, and 150 km are adopted in this study for the structural stochastic response analyses. The combinations of magnitude and distance are summarized in Table 3.

4.1. The SDOF Structural Systems

This section analyzed an SDOF system with a natural period of 3.0s for structural stochastic response analysis. First, for each magnitude-distance pair listed in Table 3, the structural maximum inter-layer relative displacement responses for every individual time series were calculated. Based on these results, the probability distribution histograms in the time series domain were plotted and compared with the PDF curves obtained in the frequency domain. In addition, CDF curves derived by integrating the probability distribution histograms in the time domain were compared with those obtained from the PDF curves in the frequency domain.

4.1.1. Comparison of PDF

As shown in Figs. 1–4, the black dashed lines represent the PDF curves obtained using the proposed approach, while the blue bars indicate the probability distribution histograms derived from time series analysis (TSA) results. It can be seen that the proposed method effectively captures both the central tendency and the spread of the maximum inter-story relative displacement response distribution. The PDF curves align closely with the probability histograms obtained from 100,000 time series simulations. In particular, under near-field conditions (R_{RUP} = 10 km and R_{RUP} = 50 km), the predictions are

Table 3. Combinations of magnitude and distance.

Distance (R_{RUP}/km)	Magnitude (M)
10	5.0, 6.0, 7.0, 8.0
50	5.0, 6.0, 7.0, 8.0
100	5.0, 6.0, 7.0, 8.0
150	5.0, 6.0, 7.0, 8.0

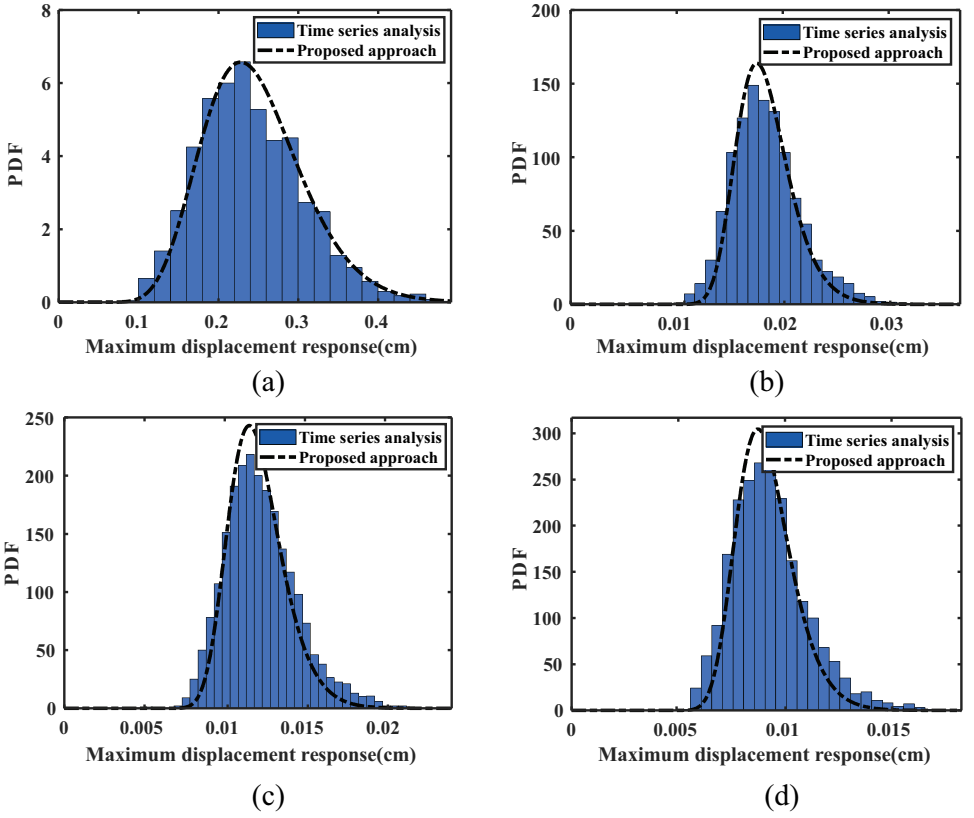

Figure 1. Comparison PDFs of maximum inter-layer relative displacements of the SDOF system under earthquakes sequentially with $M \in \{5.0, 6.0, 7.0, 8.0\}$, when R_{RUP} = 10km.

smooth and accurate across all magnitude ranges (M = 5.0–8.0), demonstrating the high reliability of the method in near-field scenarios.

As the distance increases, the proposed approach continues to provide reliable predictions for larger-magnitude events (M = 7.0 and M = 8.0), with PDF curves generally consistent with TSA results and exhibiting stable distributions. This indicates that the method remains applicable in mid-field and high-magnitude scenarios. However, at a larger distance (R_{RUP} = 150 km), for smaller-magnitude events (M = 5.0 and M = 6.0), the predicted PDFs are narrower with sharper peaks.

4.1.2. Comparison of CDF

To characterize the cumulative probabilities of the maximum inter-layer relative displacement responses at different thresholds, Figs. 5–8 present the corresponding CDF curves. In these figures, the red dashed lines and blue solid lines represent the results obtained by the proposed approach and TSA, respectively. Overall, the proposed approach is able to reproduce the cumulative probability characteristics of structural responses quite well. In particular, under shorter distance conditions (R_{RUP} = 10 km and R_{RUP} = 50 km), the predicted CDF curves show a high degree of agreement with TSA results across all magnitudes (M = 5.0–8.0), indicating the high accuracy and reliability of the method in near-field scenarios.

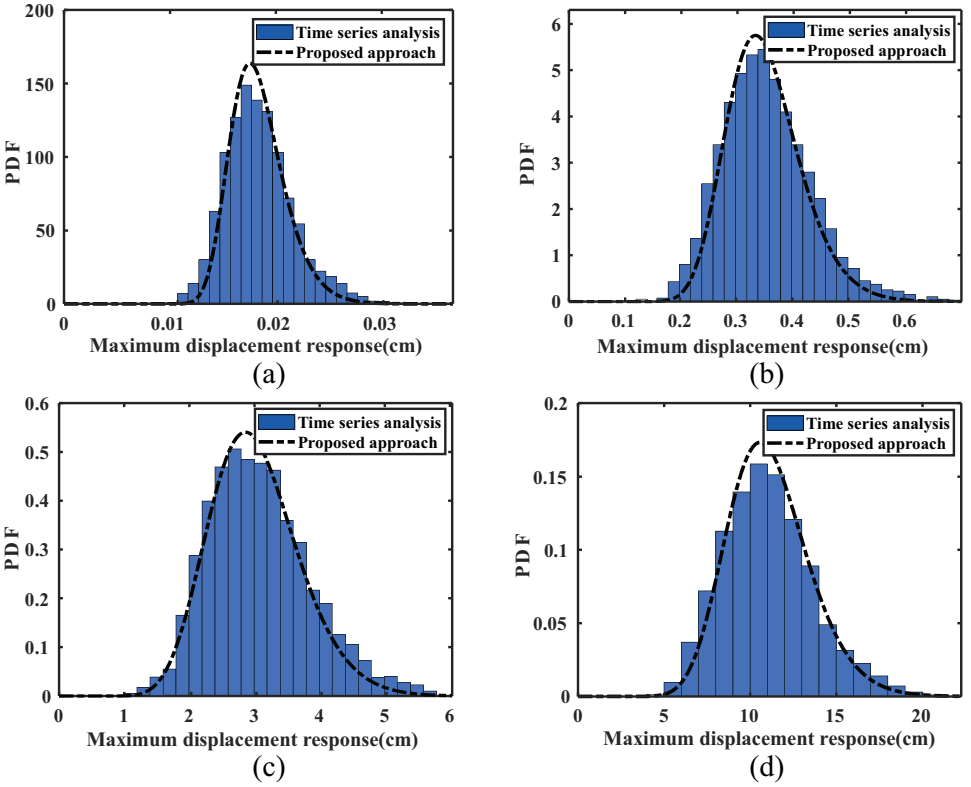

Figure 2. Comparison PDFs of maximum inter-layer relative displacements of the SDOF system under earthquakes sequentially with $M \in \{5.0, 6.0, 7.0, 8.0\}$, when R_{RUP} = 50km.

As the distance increases, especially with larger distances (R_{RUP} = 100 km and R_{RUP} = 150 km), the predicted CDFs for larger-magnitude events (M = 7.0 and M = 8.0) remain in good agreement with TSA results. However, for smaller-magnitude events (M = 5.0 and M = 6.0) at R_{RUP} = 150 km, the CDF curves from the proposed approach slightly underestimate the cumulative probability at low responses and slightly overestimate it at high thresholds, while the overall deviation remains very limited. This phenomenon is consistent with the previously noted characteristics of the PDF curves under smaller-magnitude and larger-distance conditions, where the PDF tends to exhibit an overestimated peak and an overly concentrated distribution.

To further quantify the agreement between the CDFs predicted by the proposed approach and the TSA results, the Kolmogorov–Smirnov (K-S) test was employed (Cardoso and Galeno 2023). This test measures the similarity between two distributions by calculating the maximum absolute difference (D value) between the predicted and actual CDFs, as shown in Figs. 4–8. The results show that for near-field conditions (R_{RUP} = 10 km and 50 km) and larger magnitudes (M = 7.0–8.0), the D values are generally small (approximately 0.03–0.05), indicating a high level of agreement and high prediction accuracy. For larger-distance conditions (R_{RUP} = 100 km and 150 km) and lower-magnitude events (M = 5.0–6.0), the D values increase slightly (up to 0.0941), reflecting minor deviations in the CDF predictions under these specific scenarios, although the overall agreement remains acceptable.

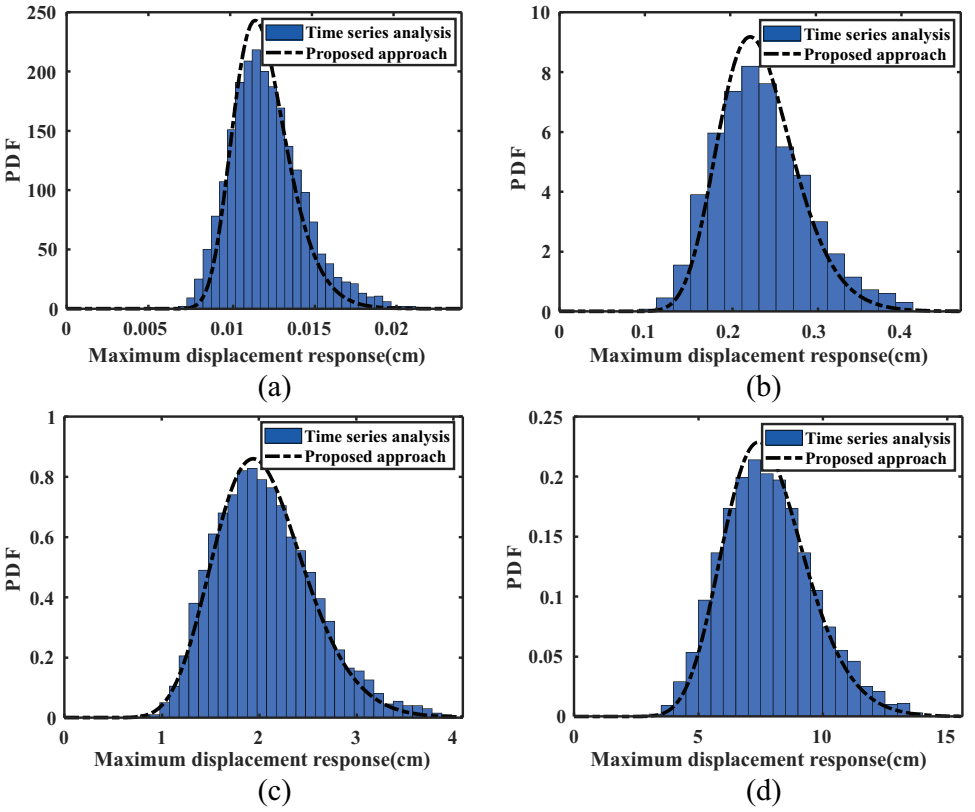

Figure 3. Comparison PDFs of maximum inter-layer relative displacements of the SDOF system under earthquakes sequentially with $M \in \{5.0, 6.0, 7.0, 8.0\}$, when R_{RUP} = 100km.

4.1.3. Comparison of Mean Value

Based on the PDF and CDF curves of maximum inter-layer relative displacement responses, the corresponding mean values of 100,000 time series were computed. The results were compared with those predicted by the proposed approach and illustrated in Fig. 9. It can be observed that the predicted values are generally distributed around the $y=x$ line, indicating a strong consistency between the two results. The calculated root mean square error (RMSE) is 0.2079, further confirming the accuracy and reliability of the proposed method in response prediction.

To further quantify the prediction accuracy, the relative errors (RE) for each magnitude-distance pair were also calculated and summarized in Table 4. The REs are generally low, indicating that the proposed method accurately predicts the statistical characteristics of structural responses. Slightly higher REs appear for smaller-magnitude and larger-distance events (M = 5.0–6.0, R_{RUP} = 100 km) but remain acceptable. For larger events (M = 7.0–8.0), errors are lower and stable across distances. Overall, mean REs range from 0.0121 to 0.0624, confirming the method's reliability and robustness.

4.1.4. Comparison of Failure Probability

Based on the maximum inter-layer relative displacement responses and the corresponding threshold specified in the relevant structural codes, cases exceeding this threshold were defined as failures. Accordingly, the failure probabilities of the SDOF system under each magnitude-

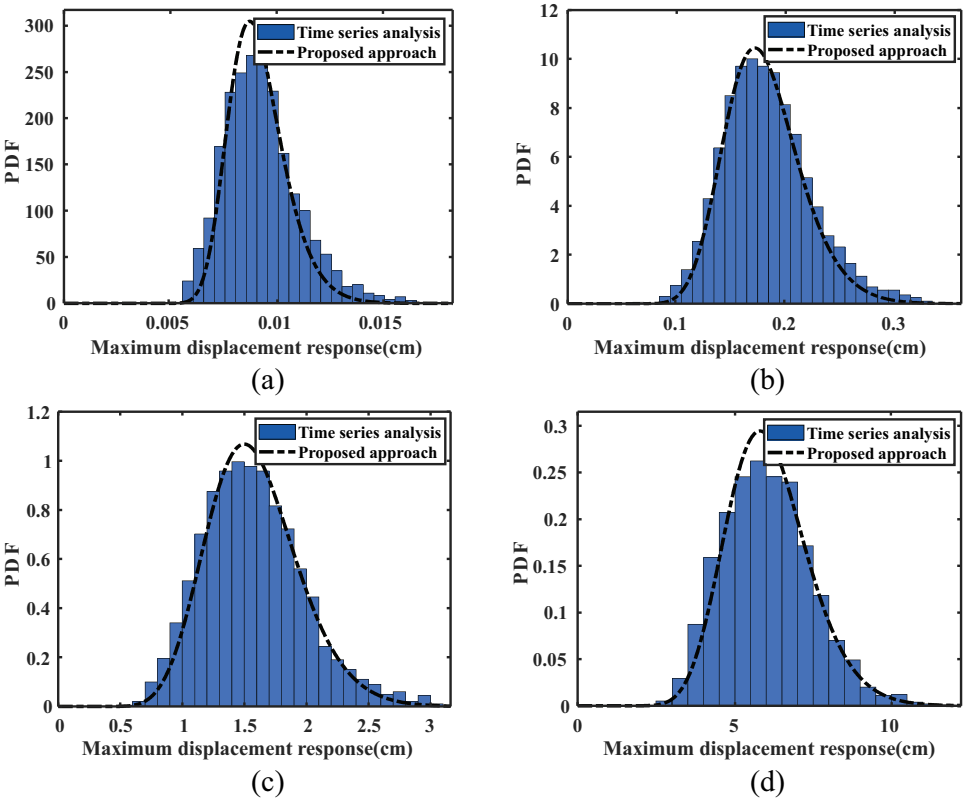

Figure 4. Comparison PDFs of maximum inter-layer relative displacements of the SDOF system under earthquakes sequentially with $M \in \{5.0, 6.0, 7.0, 8.0\}$, when R_{RUP} = 150km.

distance pair were calculated, as shown in Table 5. It can be found that the structural failure probabilities predicted by the proposed approach are in strong agreement with the results of TSA.

The analysis indicates that, compared with PDFs of time-series, the proposed method exhibits slight overestimation and concentration for smaller-magnitude and larger-distance events. This causes the corresponding CDF to be slightly underestimated at low response values. As the response increases beyond the value corresponding to the PDF peak, the predicted CDF intersects with the time-series CDF and exceeds it at higher responses. For the maximum inter-layer relative displacement, the proposed method closely matches the time-series results, indicating that the effect of PDF overestimation is negligible. However, in assessing structural failure probability, the slight overestimation of the PDF leads to underestimation at lower thresholds and overestimation at higher thresholds.

4.2. The MDOF Structural Systems

This section considers a three-degree-of-freedom structural system with mass and stiffness parameters detailed in Table 6. First, for each magnitude-distance pair listed in Table 3, the inter-layer relative displacement responses between the layers 0–1, 1–2, and 2–3 were calculated and the maximum responses of each inter-layer were identified under every individual time series. According to the results of 100,000 time series, the corresponding probability distribution histograms of each inter-layer were plotted and compared with the PDF curves obtained in the frequency domain. In addition, CDF curves derived by integrating the probability distribution histograms in the time domain were compared with those obtained from the PDF curves in the frequency domain.

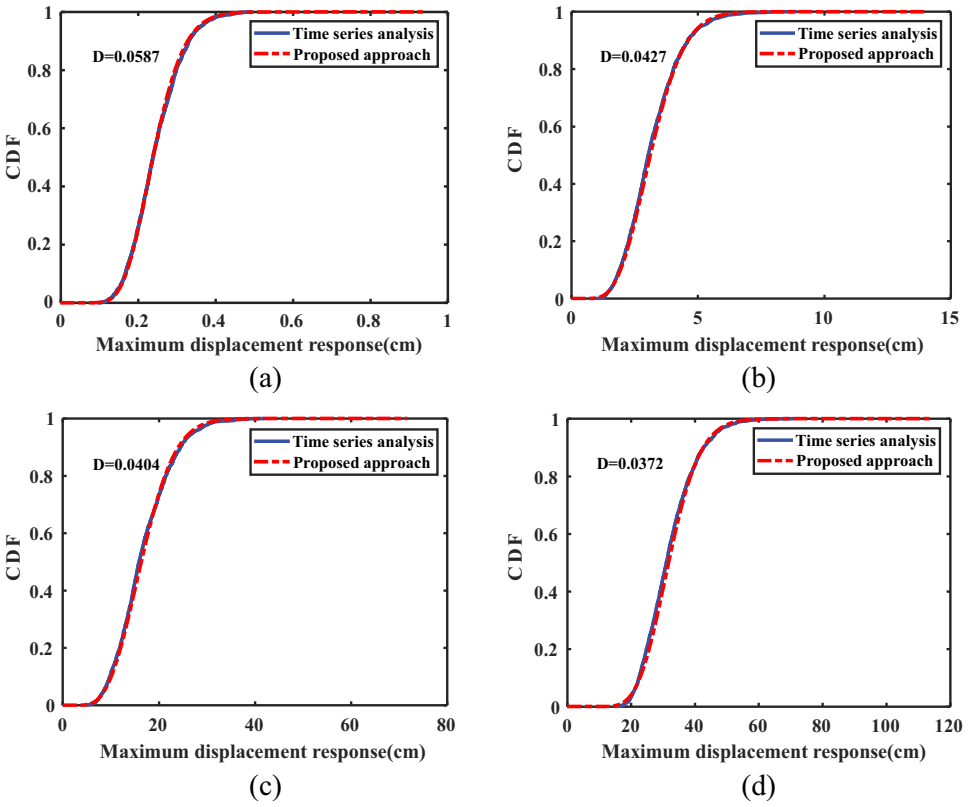

Figure 5. Comparison CDFs of maximum inter-layer relative displacements of the SDOF system under earthquakes sequentially with $M \in \{5.0, 6.0, 7.0, 8.0\}$, when R_{RUP} = 10km.

4.2.1. Comparison of PDF

As shown in Figs. 10–13, the black dashed lines represent the PDF curves obtained by the proposed approach, while the blue bars indicate the probability distribution histograms derived from TSA. In each figure, the comparison results for layers 0–1, 1–2, and 2–3 are presented sequentially from left to right. The results indicate that the proposed approach can effectively capture the shape, central tendency, and dispersion characteristics of the maximum inter-layer relative displacement response distribution, particularly under near-field conditions ($R_{RUP} = 10$ km and 50 km). For other distance categories ($R_{RUP} = 100$ km and 150 km), the proposed approach still shows good agreement with TSA results for larger-magnitude events (M = 7.0–8.0). However, for lower-magnitude events (M = 5.0–6.0), the PDF curves predicted by the proposed approach become narrower and sharper, leading to slight overestimation near the medium response levels and underestimation at smaller and larger response levels.

4.2.2. Comparison of CDF

To characterize the cumulative probability distribution of the maximum inter-layer relative displacement responses of the MDOF systems at different thresholds, the CDF curves for each magnitude-distance pair are plotted in Figs. 14-17. In each figure, the results for inter-layers 0–1, 1–2, and 2–3 are presented from left to right. As shown in the figures, the CDF curves predicted by the proposed

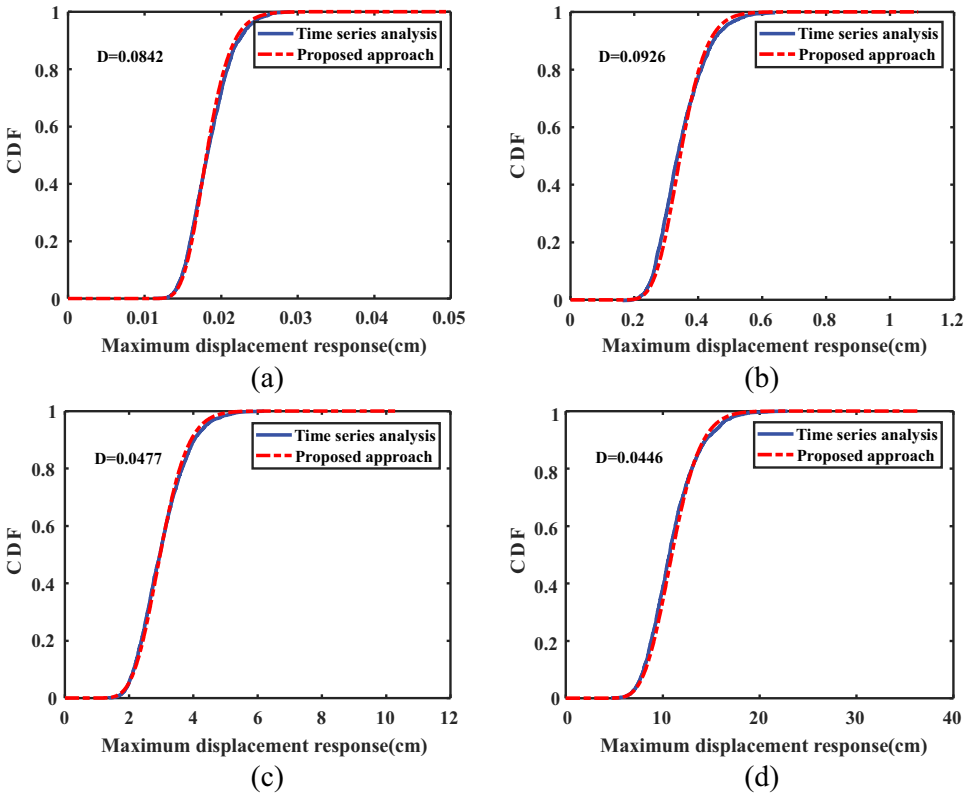

Figure 6. Comparison CDFs of maximum inter-layer relative displacements of the SDOF system under earthquakes sequentially with $M \in \{5.0, 6.0, 7.0, 8.0\}$, when R_{RUP} = 50km.

method exhibit good overall agreement with the TSA results, particularly under shorter distance conditions (R_{RUP} = 10 km and 50 km), indicating that the proposed method can accurately capture the cumulative probability characteristics of the structural responses. For larger-distance conditions (R_{RUP} = 100 km and 150 km), slight deviations are observed between the predicted and TSA curves, mainly manifesting as higher cumulative probabilities at larger response levels and lower probabilities at smaller response levels. This phenomenon is more pronounced for lower-magnitude events (M = 5.0–6.0), which is consistent with the corresponding PDF overestimation.

To verify the applicability of the proposed method in the MDOF case, the K-S test was employed to compare the CDFs predicted by the proposed method with those from TSA, and the resulting D values are shown in Figs. 14–17. The D values across different magnitude-distance pairs remain small (mostly 0.02–0.09), indicating strong consistency between the predicted and time-domain CDFs. Slightly higher D values are observed for smaller-magnitude and larger distance cases (M = 5.0–6.0, R_{RUP} = 100 km and 150 km), while for moderate-to-large magnitudes (M = 7.0–8.0) the D values remain consistently low. Overall, the results confirm that the proposed method accurately captures the cumulative probability characteristics of structural responses in MDOF systems.

4.2.3. Comparison of Mean Value

Based on the PDF and CDF curves, the mean values across 100,000 time series were calculated and compared with those of the maximum inter-layer relative displacement responses obtained by the proposed approach. The results were compared with those predicted by the proposed approach and

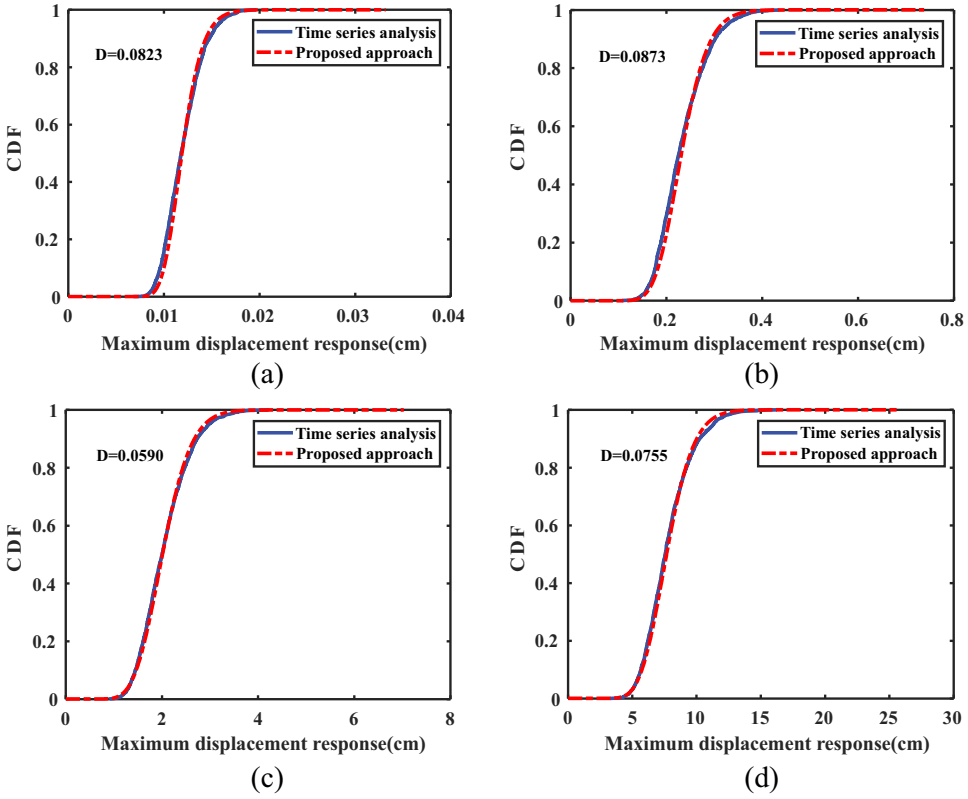

Figure 7. Comparison CDFs of maximum inter-layer relative displacements of the SDOF system under earthquakes sequentially with $M \in \{5.0, 6.0, 7.0, 8.0\}$, when R_{RUP} = 100km.

illustrated in Fig. 18. It can be observed that the predicted values are generally distributed around the line of $y=x$, with RMSE of only 0.2153, 0.0973, and 0.1191, indicating a strong consistency between the two results.

To further quantify the prediction accuracy, the REs for each magnitude-distance pair were also calculated and summarized in Table 7. Based on the results, the RE of each inter-layer across different magnitude-distance pair remains low, indicating accurate prediction of the statistical characteristics of MDOF structural responses. Slightly higher REs are observed for low-magnitude events (M = 5.0–6.0) and the first inter-story layer, likely due to smaller response amplitudes and greater variability, but the mean errors remain below 0.13. These results confirm the high accuracy and stability of the proposed method across different magnitudes, distances, and inter-layer positions.

4.2.4. Comparison of Failure Probability

According to the maximum inter-layer relative displacement responses and the relevant structural codes, the failure probabilities of the MDOF system under each magnitude-distance pair were calculated and shown in Table 8. It can be observed that the failure probabilities obtained by the proposed approach align well with the results in the time series domain. Similar to the SDOF case, the proposed method slightly overestimates the PDF of responses for smaller-magnitude and larger-distance events, causing minor underestimation of the CDF at low responses and slight overestimation at high responses. For the maximum inter-layer relative displacement, the method remains in close

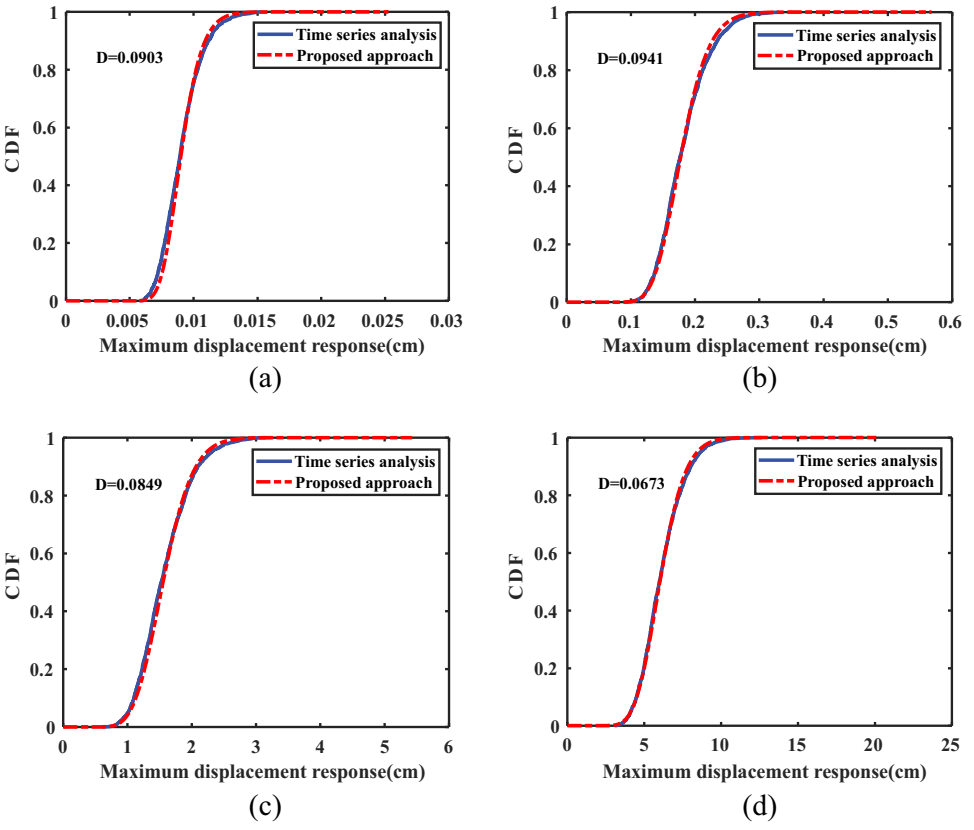

Figure 8. Comparison CDFs of maximum inter-layer relative displacements of the SDOF system under earthquakes sequentially with $M \in \{5.0, 6.0, 7.0, 8.0\}$, when $R_{RUP} = 150$km.

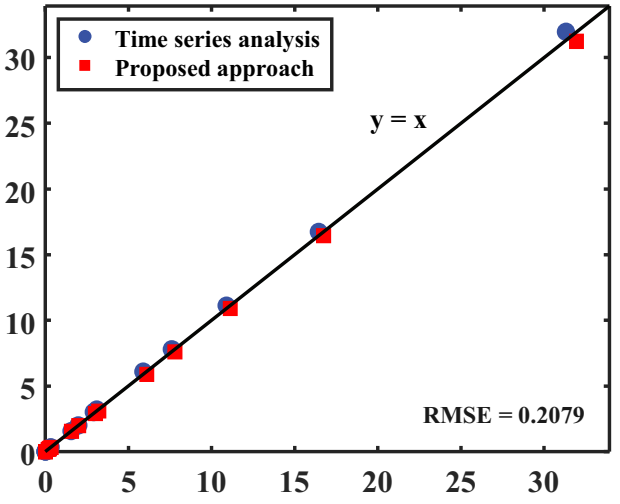

Figure 9. Comparison of mean response values between time series analysis and proposed approach.

Table 4. RE values of the mean maximum inter-layer relative displacement responses under each magnitude-distance pair.

Magnitude	R_{RUP}=10km	R_{RUP}=50km	R_{RUP}=100km	R_{RUP}=150km	Mean
M=5.0	0.0363	0.0401	0.0431	0.0341	0.0384
M=6.0	0.0376	0.0598	0.0567	0.0624	0.0541
M=7.0	0.0185	0.0368	0.0136	0.0161	0.0213
M=8.0	0.0309	0.0121	0.0261	0.0362	0.0263
Mean	0.0308	0.0372	0.0349	0.0372	0.0351

Table 5. Failure probabilities of the SDOF system under each magnitude-distance pair.

Magnitude	Method	R_{RUP}=10km	R_{RUP}=50km	R_{RUP}=100km	R_{RUP}=150km
M=5.0	Proposed approach	0	0	0	0
	TSA	0	0	0	0
M=6.0	Proposed approach	0.2824	0	0	0
	TSA	0.2930	0	0	0
M=7.0	Proposed approach	1	0.0519	0	0
	TSA	1	0.0580	0	0
M=8.0	Proposed approach	1	1	0.9906	0.9086
	TSA	1	1	0.9880	0.8970

Table 6. Parameters of the MDOF system.

Structure	Layer 1	Layer 2	Layer 3
Mass (kg)	200	200	100
Stiffness (N/m)	20000	20000	10000

agreement with time-series results. As a result of PDF overestimation, the predicted structural failure probability is slightly underestimated at low thresholds and slightly overestimated at high thresholds.

The results from both two case studies indicate that the proposed approach exhibits slight overestimation and concentration in the predicted PDFs for smaller-magnitude and larger-distance events. This phenomenon may be primarily attributed to two reasons: On the one hand, the duration model adopted in the proposed approach is not fully consistent with the actual duration of the time series, introducing a certain degree of approximation. On the other hand, the verification criterion for the ground motion generation based on the FAS model ensures consistency between the mean time-history spectrum and the target FAS, but it does not guarantee that each individual time history strictly follows the same statistical distribution. Consequently, although the proposed method achieves good agreement with the time-series results in terms of the mean maximum inter-layer displacement and structural failure probability, it is less capable of reproducing localized peaks observed in some time histories, leading to a relatively more concentrated predicted PDF, which could be further improved in future studies.

5. Conclusions

This study proposed an end-to-end analytical framework for stochastic structural response analysis, which directly simulates the entire process from specific seismic source conditions to structural responses in the frequency domain, achieving a physical coupling between ground motion modeling and structural response analysis. Within the proposed framework, a source-based FAS model, which has been thoroughly verified using real seismic records, coupled with a ground motion duration model, is employed to capture the entire seismic wave propagation process – from earthquake generation to arrival at the ground surface. These models can represent any seismic sources of interest

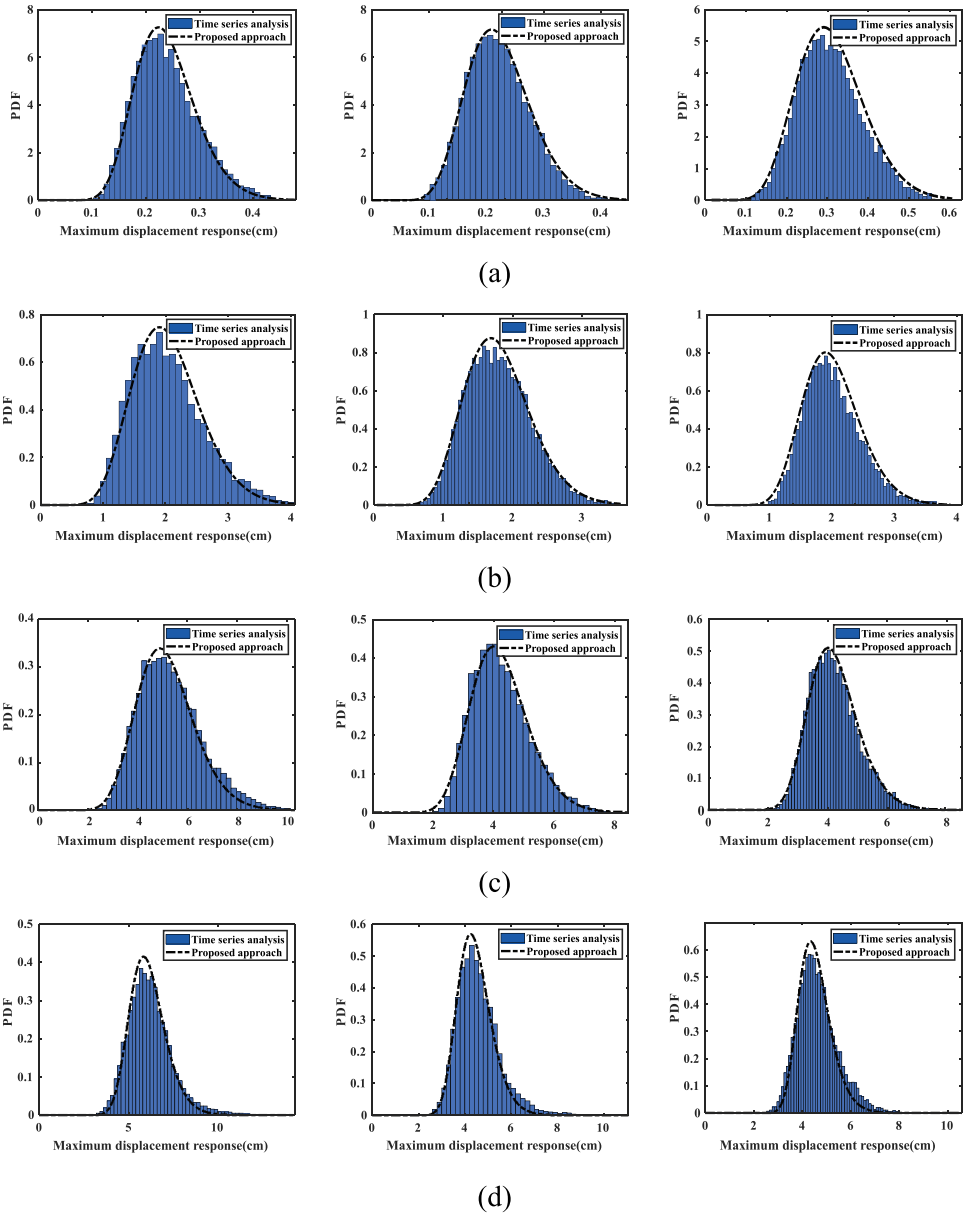

Figure 10. Comparison PDFs of maximum inter-layer (0–1, 1–2 and 2–3) relative displacements of the MDOF system under earthquakes sequentially with $M \in \{5.0, 6.0, 7.0, 8.0\}$, when R_{RUP} = 10km.

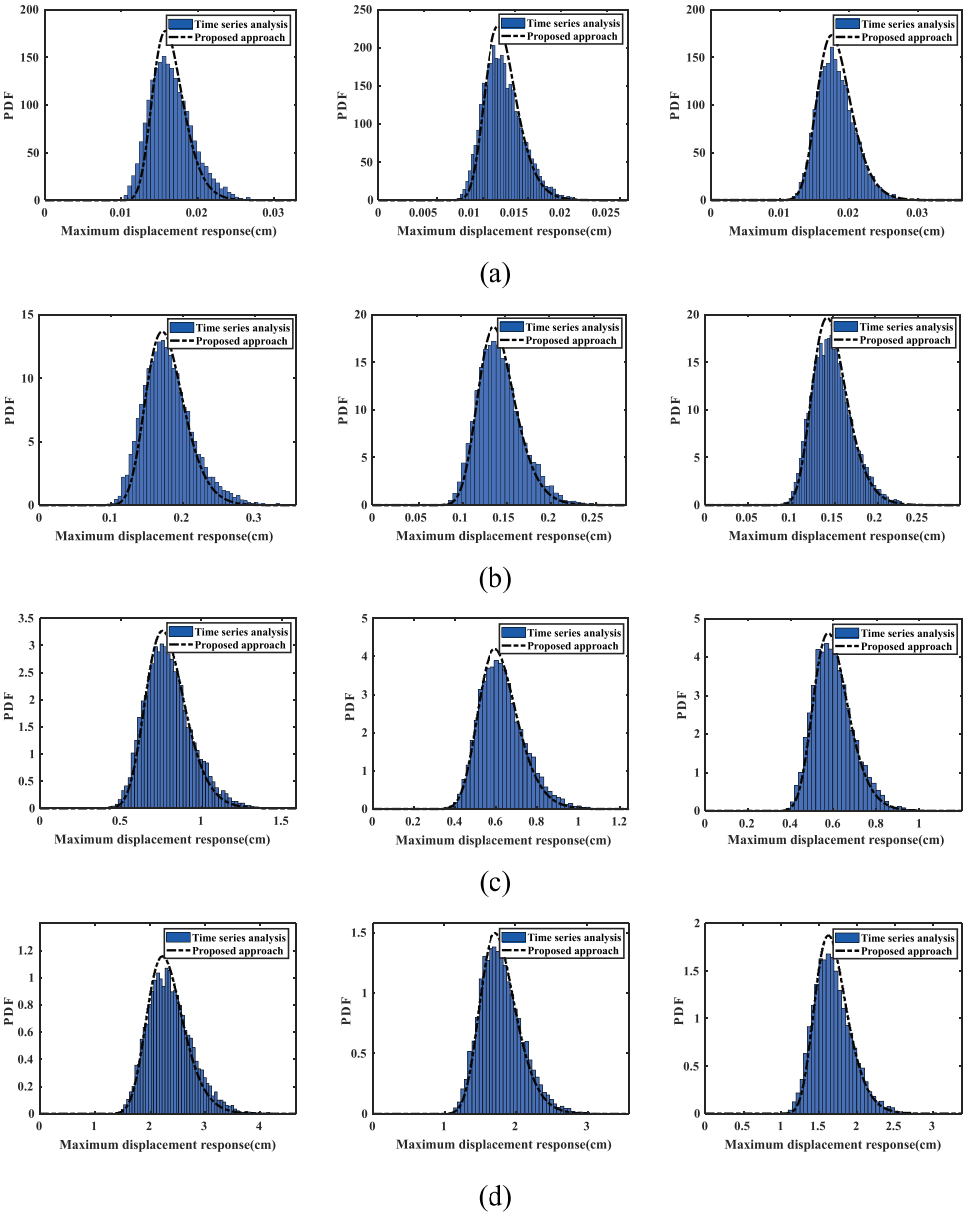

Figure 11. Comparison PDFs of maximum inter-layer (0–1, 1–2 and 2–3) relative displacements of the MDOF system under earthquakes sequentially with $M \in \{5.0, 6.0, 7.0, 8.0\}$, when $R_{RUP} = 50$km.

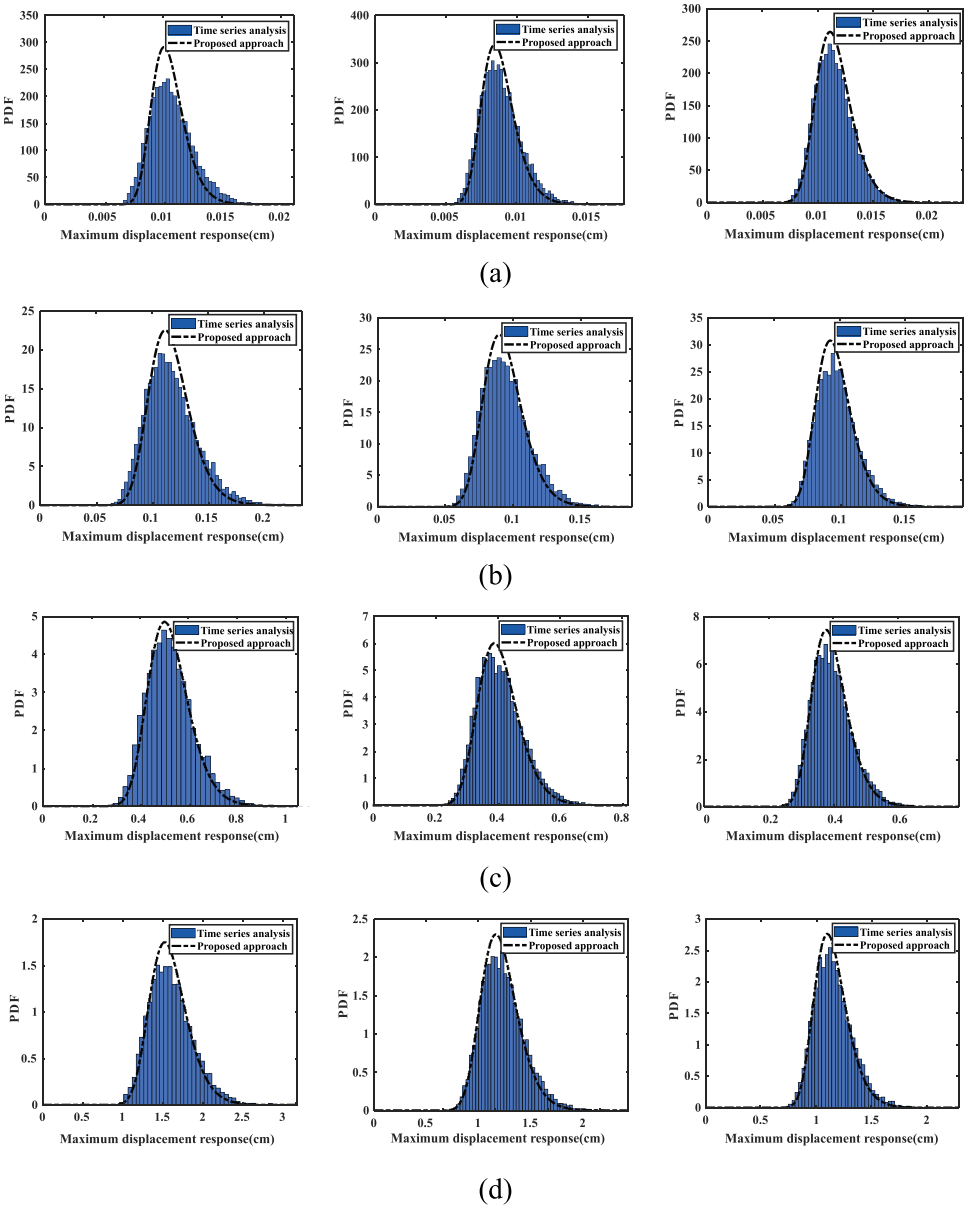

Figure 12. Comparison PDFs of maximum inter-layer (0–1, 1–2, and 2–3) relative displacements of the MDOF system under earthquakes sequentially with $M \in \{5.0, 6.0, 7.0, 8.0\}$, when $R_{RUP} = 100$km.

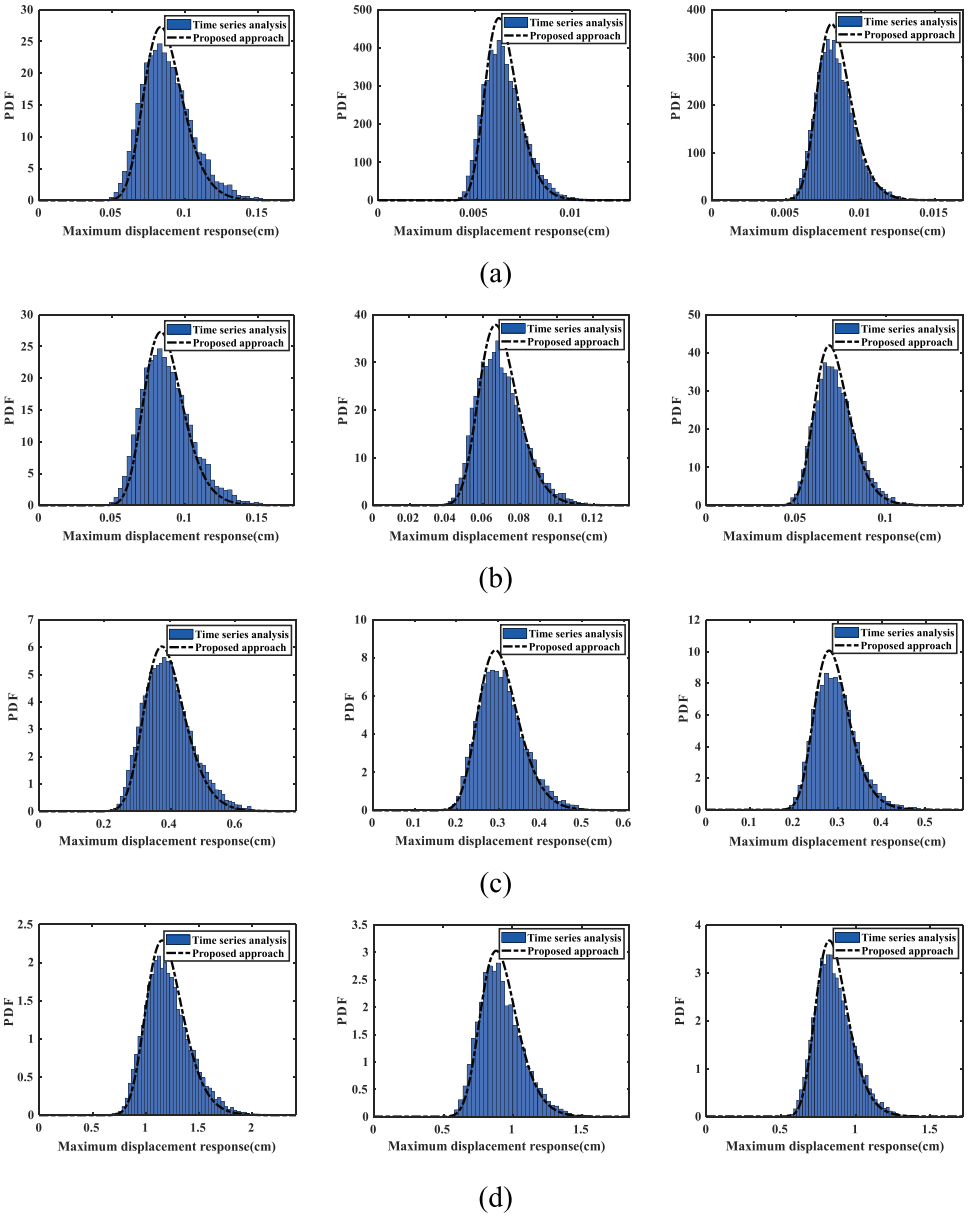

Figure 13. Comparison PDFs of maximum inter-layer (0–1, 1–2 and 2–3) relative displacements of the MDOF system under earthquakes sequentially with $M \in \{5.0, 6.0, 7.0, 8.0\}$, when R_{RUP} = 150km.

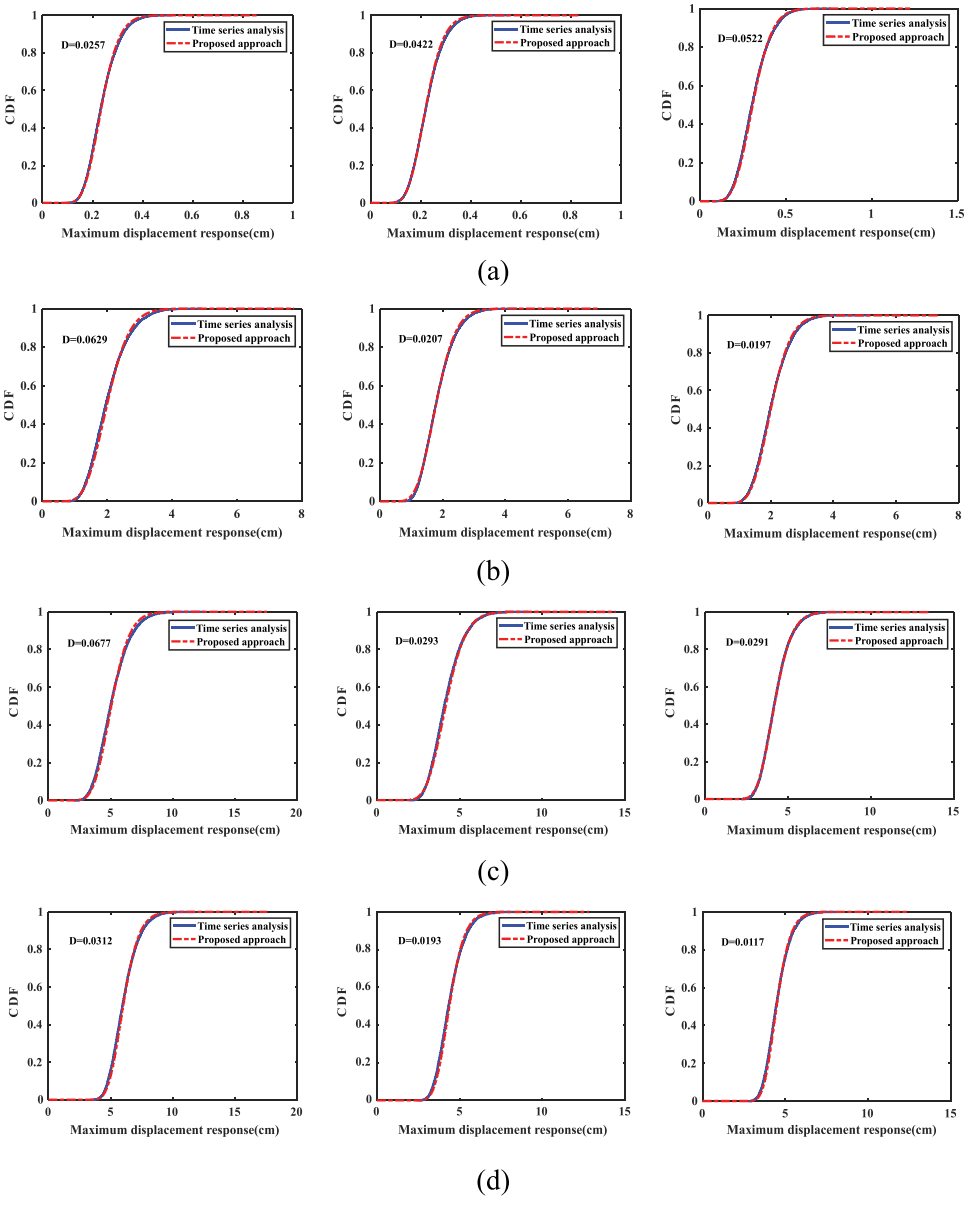

Figure 14. Comparison CDFs of maximum inter-layer (0–1, 1–2, and 2–3) relative displacements of the MDOF system under earthquakes sequentially with $M \in \{5.0, 6.0, 7.0, 8.0\}$, when R_{RUP} = 10km.

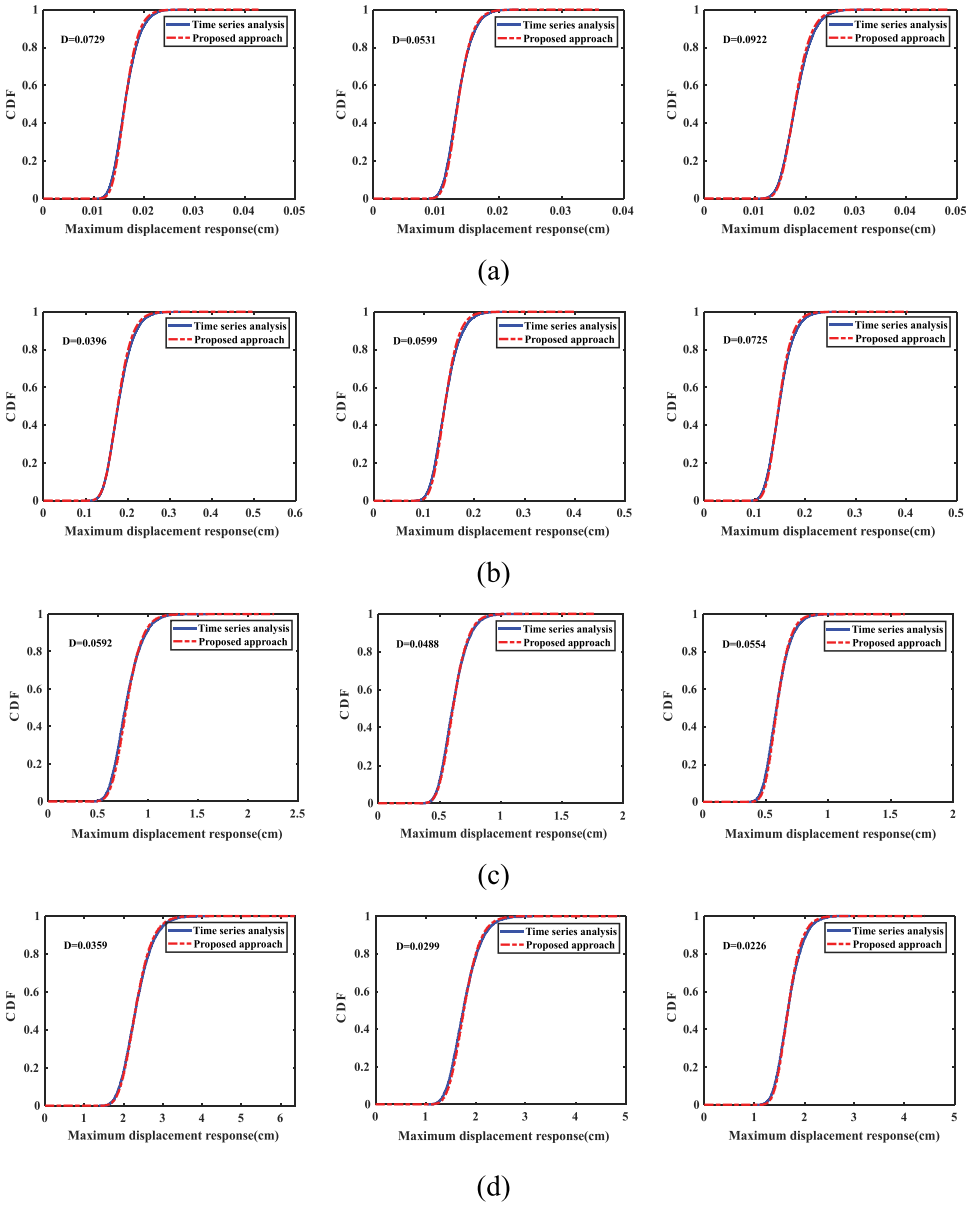

Figure 15. Comparison CDFs of maximum inter-layer (0–1, 1–2, and 2–3) relative displacements of the MDOF system under earthquakes sequentially with $M \in \{5.0, 6.0, 7.0, 8.0\}$, when $R_{RUP} = 50$km.

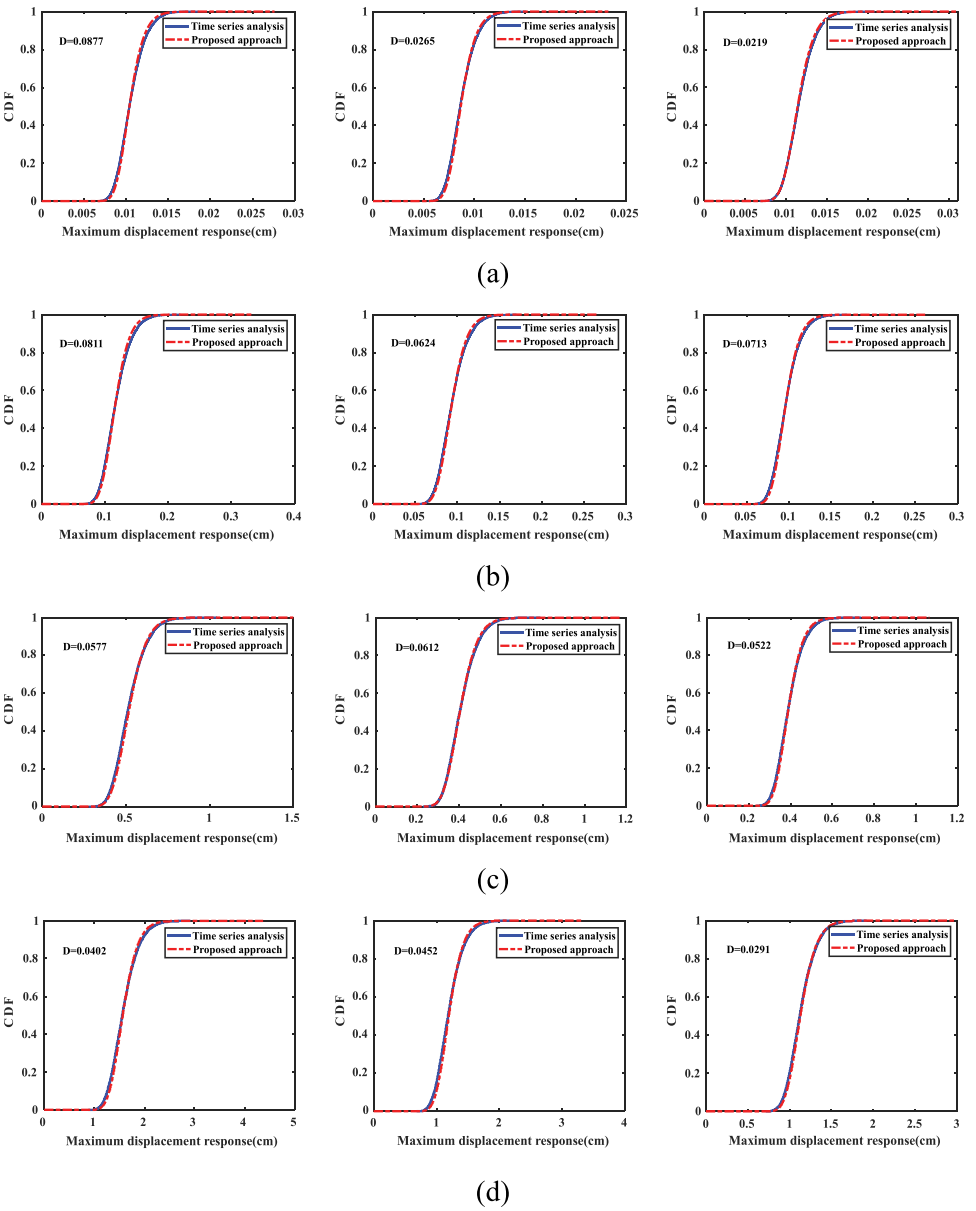

Figure 16. Comparison CDFs of maximum inter-layer (0–1, 1–2, and 2–3) relative displacements of the MDOF system under earthquakes sequentially with $M \in \{5.0, 6.0, 7.0, 8.0\}$, when R_{RUP} = 100km.

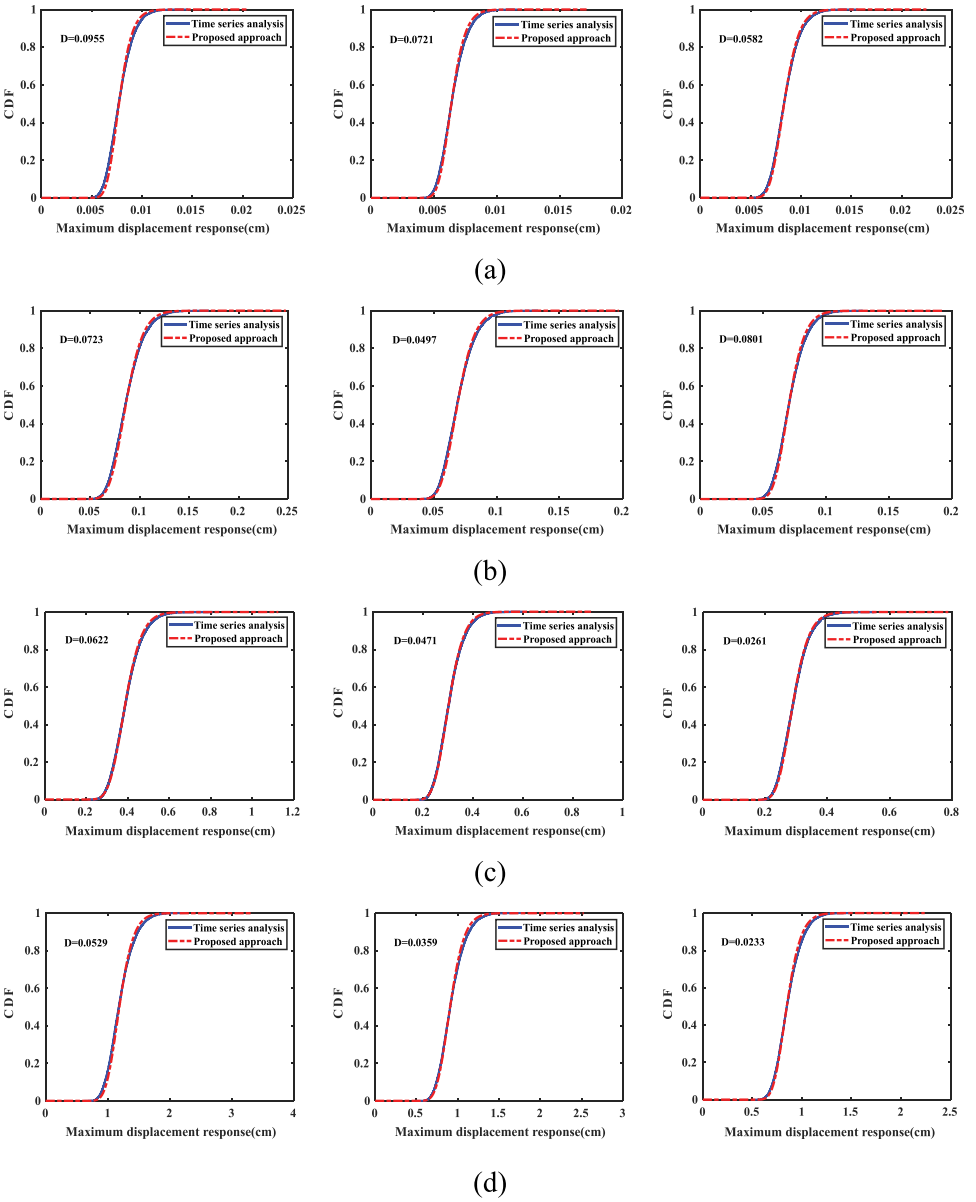

Figure 17. Comparison CDFs of maximum inter-layer (0–1, 1–2, and 2–3) relative displacements of the MDOF system under earthquakes sequentially with $M \in \{5.0, 6.0, 7.0, 8.0\}$, when R_{RUP} = 150km.

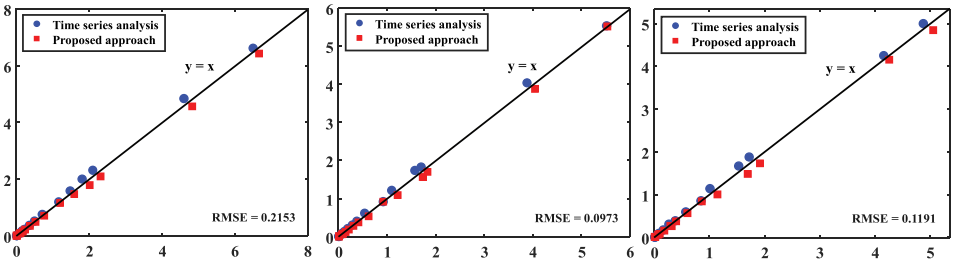

Figure 18. Comparison of mean response values between time series analysis and proposed approach.

Table 7. RE values of the mean maximum inter-layer relative displacement responses under each magnitude-distance pair.

Magnitude	Inter-layer	R_{RUP}=10km	R_{RUP}=50km	R_{RUP}=100km	R_{RUP}=150km	Mean
M=5.0	0–1	0.0551	0.0781	0.0816	0.0833	0.0745
	1–2	0.1252	0.1225	0.1102	0.0911	0.1112
	2–3	0.1074	0.1042	0.1018	0.0374	0.0877
M=6.0	0–1	0.1102	0.0927	0.1031	0.0445	0.0876
	1–2	0.0752	0.0953	0.0716	0.0645	0.0776
	2–3	0.0948	0.0987	0.1301	0.0608	0.0961
M=7.0	0–1	0.0922	0.0725	0.0551	0.0434	0.0658
	1–2	0.0655	0.1255	0.0854	0.0683	0.0861
	2–3	0.0237	0.0493	0.0382	0.0594	0.0426
M=8.0	0–1	0.1011	0.0721	0.0759	0.0347	0.0709
	1–2	0.0027	0.1033	0.1102	0.0028	0.0547
	2–3	0.0463	0.0788	0.0924	0.0175	0.0587
Mean	0–1	0.0919	0.0785	0.0789	0.0514	0.0751
	1–2	0.0672	0.1116	0.0923	0.0566	0.0819
	2–3	0.0681	0.0884	0.0906	0.0437	0.0727

Table 8. Failure probabilities of the MDOF system under each magnitude-distance pair.

Magnitude	Method	R_{RUP}=10km	R_{RUP}=50km	R_{RUP}=100km	R_{RUP}=150km
M=5.0	Proposed approach	0.0066	0	0	0
	TSA	0.0059	0	0	0
M=6.0	Proposed approach	1	0	0	0
	TSA	1	0	0	0
M=7.0	Proposed approach	1	0.9991	0.3461	0.0142
	TSA	1	0.9100	0.2560	0.0400
M=8.0	Proposed approach	1	1	1	1
	TSA	1	1	1	1

in earthquake engineering and then serve as the inputs for stochastic response analyses of structures in both frequency and time series domains. The main contributions of this study are summarized as follows:

(1) Compared with traditional spectral models considering only site effects, the proposed approach incorporates additional seismic parameters to quantify the influences of seismic source, propagation path, and site effects, thereby providing a more comprehensive and intuitive characterization of structural responses with varying seismic characteristics.
(2) Analytical formulations for the frequency-domain stochastic response of MDOF systems are derived, which can also be extended to time-domain analysis by converting the FAS to time

series, thereby preserving both the computational efficiency in frequency domain and the accuracy in time series domain.

(3) Numerical examples are conducted using the proposed approach to evaluate stochastic responses and failure probabilities under varying magnitudes and distances. The results show a high level of agreement with time-domain analyses, thereby demonstrating its feasibility and accuracy across different structural systems and source conditions.

Acknowledgments

This study was partially supported by the National Key R&D Program of China (2023YFC3805100, 2023YFC3805101) and the Japan Society for the Promotion of Science (JSPS) KAKENHI (Grant No. 24K17336). This study used strong-motion records from K-NET and KiK-net. The authors are grateful for the financial supports and earthquake data.

Author Contributions

CRediT: **Dengke Jiu:** Formal analysis, Software, Validation, Visualization, Writing – original draft; **Haizhong Zhang:** Funding acquisition, Methodology, Supervision, Writing – review & editing; **Yan-Gang Zhao:** Funding acquisition, Resources, Supervision, Writing – review & editing.

Disclosure Statement

No potential conflict of interest was reported by the author(s).

Funding

This study was partially funded by the National Key R&D Program of China [2023YFC3805100, 2023YFC3805101] and the Japan Society for the Promotion of Science (JSPS) KAKENHI [Grant No. 24K17336].

Code Availability

Available upon request.

Data Availability Statement

All data generated or analyzed during this study are included in this published article.

References

Abdelnaby, A. E., and A. S. Elnashai. 2014. "Performance of Degrading Reinforced Concrete Frame Systems Under the Tohoku and Christchurch Earthquake Sequences." *Journal of Earthquake Engineering* 18 (7): 1009–1036. https://doi.org/10.1080/13632469.2014.923796.

Atkinson, G. M., and D. M. Boore. 1995. "Ground-Motion Relations for Eastern North America." *Bulletin of the Seismological Society of America* 85 (1): 17–30. https://doi.org/10.1785/BSSA0850010017.

Atkinson, G. M., and D. M. Boore. 2014. "The Attenuation of Fourier Amplitudes for Rock Sites in Eastern North America." *Bulletin of the Seismological Society of America* 104 (1): 513–528. https://doi.org/10.1785/0120130136.

Beresnev, I., and G. M. Atkinson. 1998. "FINSIM: A FORTRAN Program for Simulating Stochastic Acceleration Time Histories from Finite Faults." *Seismological Research Letters* 69 (1): 27–32. https://doi.org/10.1785/gssrl.69.1.27.

Boore, D. M. 1983. "Stochastic Simulation of High-Frequency Ground Motions Based on Seismological Models of the Radiated Spectra." *Bulletin of the Seismological Society of America* 73 (6A): 1865–1894.

Boore, D. M. 2000. *SMSIM–Fortran Programs for Simulating Ground Motions from Earthquakes: Version 2.0.–A Revision of OFR 96-80-A* (No. 2000-509). US Geological Survey.

Boore, D. M. 2003. "Simulation of Ground Motion Using the Stochastic Method." *Pure and Applied Geophysics* 160 (3): 635–676. https://doi.org/10.1007/PL00012553.
Boore, D. M. 2005. *SMSIM. FORTRAN Programs for Simulating Ground Motions from Earthquakes: Version 2.3 a Revision of OFR 96-80-A*. U.S. Geol. Surv. Open-File Rept. (A Modified Version of OFR 00-509, 5 [Version 2.30]).
Boore, D. M. 2009. "Comparing Stochastic Point-Source and Finite-Source Ground-Motion Simulations: SMSIM and EXSIM." *Bulletin of the Seismological Society of America* 99 (6): 3202–3216. https://doi.org/10.1785/0120090056.
Boore, D. M. 2015. Point-Source Stochastic-Method Simulations of Ground Motions for the PEER NGA-East Project. *USGS Report*, 11–49.
Boore, D. M., and W. B. Joyner. 1997. "Site Amplifications for Generic Rock Sites." *Bulletin of the Seismological Society of America* 87 (2): 327–341. https://doi.org/10.1785/BSSA0870020327.
Boore, D. M., and E. M. Thompson. 2012. "Empirical Improvements for Estimating Earthquake Response Spectra with Random-Vibration Theory." *Bulletin of the Seismological Society of America* 102 (2): 761–772. https://doi.org/10.1785/0120110244.
Boore, D. M., and E. M. Thompson. 2014. "Path Durations for Use in the Stochastic-Method Simulation of Ground Motions." *Bulletin of the Seismological Society of America* 104 (5): 2541–2552. https://doi.org/10.1785/0120140058.
Boore, D. M., and E. M. Thompson. 2015. "Revisions to Some Parameters Used in Stochastic-Method Simulations of Ground Motion." *Bulletin of the Seismological Society of America* 105 (2A): 1029–1041. https://doi.org/10.1785/0120140281.
Brune, J. N. 1970. "Tectonic Stress and the Spectra of Seismic Shear Waves from Earthquakes." *Journal of Geophysical Research* 75 (26): 4997–5009. https://doi.org/10.1029/JB075i026p04997.
Brune, J. N. 1971. "Correction." *Journal of Geophysical Research* 76 (20): 5002.
Calvi, G. M., and G. Andreotti. 2022. "Effects of Local Soil, Magnitude and Distance on Empirical Response Spectra for Design." *Journal of Earthquake Engineering* 26 (3): 1–28. https://doi.org/10.1080/13632469.2019.1703847.
Cardoso, D. O., and T. D. Galeno. 2023. "Online Evaluation of the Kolmogorov–Smirnov Test on Arbitrarily Large Samples." *Journal of Computational Science* 67:101959. https://doi.org/10.1016/j.jocs.2023.101959.
Cartwright, D. E., and M. S. Longuet-Higgins. 1956. "The Statistical Distribution of the Maxima of a Random Function." *Proceedings of the Royal Society of London. Series A. Mathematical and Physical Sciences* 237 (1209): 212–232.
Clough, R. W., and J. Penzien. 1975. *Dynamics of Structures*. New York: McGraw-Hill Book Co.
Ding, Y., Y. Peng, and J. Li. 2018. "A Stochastic Semi-Physical Model of Seismic Ground Motions in Time Domain." *Journal of Earthquake and Tsunami* 12 (3): 1850006. https://doi.org/10.1142/S1793431118500069.
Ding, Y., Y. Xu, and H. Miao. 2022. "A Seismic Checking Method of Engineering Structures Based on the Stochastic Semi-Physical Model of Seismic Ground Motions." *Buildings* 12 (4): 488. https://doi.org/10.3390/buildings12040488.
Estêvão, J. M., and A. Carvalho. 2015. "The Role of Source and Site Effects on Structural Failures Due to Azores Earthquakes." *Engineering Failure Analysis* 56:429–440. https://doi.org/10.1016/j.engfailanal.2014.12.010.
Filiatrault, A., D. Perrone, R. J. Merino, and G. M. Calvi. 2018. "Performance-Based Seismic Design of Nonstructural Building Elements." *Journal of Earthquake Engineering* 25 (2): 1–33. https://doi.org/10.1080/13632469.2018.1512910.
Hanks, T. C., and R. K. McGuire. 1981. "The Character of High-Frequency Strong Ground Motion." *Bulletin of the Seismological Society of America* 71 (6): 2071–2095. https://doi.org/10.1785/BSSA0710062071.
Hu, H., G. Gan, Y. Bao, X. Guo, M. Xiong, X. Han, and L. Wang. 2023. "Nonlinear Stochastic Seismic Response Analysis of Three-Dimensional Reinforced Concrete Piles." *Buildings* 13 (1): 89.
Hu, Y. X., and X. Y. Zhou. 1962. "Statistical Theory Evaluation of Earthquake Forces." *Seismic Engineering Research Reports, Vol. 1, Institute of Civil Engineering and Architecture, Chinese Academy of Sciences*, 21–32. Beijing: Science Press. (in Chinese).
Kanai, K. 1962. "On the Spectrum of Strong Earthquake Motions." *Bulletin of the Earthquake Research Institute* 40 (1): 71–90. https://doi.org/10.15083/0000033795.
Khansefid, A., and A. Bakhshi. 2022. "New Model for Simulating Random Synthetic Stochastic Earthquake Scenarios." *Journal of Earthquake Engineering* 26 (2): 1072–1089. https://doi.org/10.1080/13632469.2019.1699207.
Kottke, A. R., and E. M. Rathje. 2013. "Comparison of Time Series and Random-Vibration Theory Site-Response Methods." *Bulletin of the Seismological Society of America* 103 (3): 2111–2127. https://doi.org/10.1785/0120120254.
Li, H., and C. Chen. 2014. "A Modified Kanai-Tajimi Spectral Model for the Stationary Earthquake Induced Ground Motion Process." *Engineering Mechanics* 31 (2): 158–163. (in Chinese).
Li, J., and G. Q. Li. 1998. *Introduction to Earthquake Engineering*. Beijing: Seismological Press.
Liu, Z., W. Liu, and Y. Peng. 2016. "Random Function Based Spectral Representation of Stationary and Non-stationary Stochastic Processes." *Probabilistic Engineering Mechanics* 45:115–126. https://doi.org/10.1016/j.probengmech.2016.04.004.
Luo, C., and Y. Peng. 2024. "Stochastic Simulation of Earthquake Ground Motions Based on Improved Finite-Fault Model." *Soil Dynamics and Earthquake Engineering* 176:108336. https://doi.org/10.1016/j.soildyn.2023.108336.

Ma, C., Y. Zhang, Y. Zhao, P. Tan, and F. Zhou. 2011. "Stochastic Seismic Response Analysis of Base-Isolated High-Rise Buildings." *Procedia Engineering* 14:2468–2474. https://doi.org/10.1016/j.proeng.2011.07.310.

Meimandi-Parizi, A., A. Mahdavian, and H. Saffari. 2023. "New Empirical Equations for Determination of Fourier Amplitude Spectrum of Acceleration." *Journal of Earthquake Engineering* 27 (10): 2775–2795. https://doi.org/10.1080/13632469.2022.2133031.

Morikawa, N., A. Iwaki, H. Fujiwara, S. Akiyama, T. Maeda, H. Kubo, S. Aoi, et al. 2024. *Flat File of K-NET and KiK-Net Strong-Motion Records*, *Proceedings in the 18th World Conference on Earthquake Engineering* Tokyo, Japan: International Association for Earthquake Engineering.

Naserieh, S., H. Ghofrani, J. Shoja-Taheri, M. Dezvareh, and H. Mirzaei Alavijeh. 2022. "Strong Ground-Motion Characteristics Observed in the November 12, 2017, M 7.3 Sarpol-e Zahab, Iran Earthquake." *Journal of Earthquake Engineering* 26 (7): 3488–3505. https://doi.org/10.1080/13632469.2020.1806950.

O'Reilly, G. J., and T. J. Sullivan. 2017. "Modeling Techniques for the Seismic Assessment of the Existing Italian RC Frame Structures." *Journal of Earthquake Engineering* 23 (8): 1262–1296. https://doi.org/10.1080/13632469.2017.1360224.

Ou, J. P., D. T. Niu, and X. L. Du. 1991. "Random Earthquake Ground Motion Model and Its Parameter Determination Used in Aseismic Design." *Earthquake Engineering and Engineering Vibration* 11 (3): 45–54.

Peng, Y., Z. Mei, and J. Li. 2014. "Stochastic Seismic Response Analysis and Reliability Assessment of Passively Damped Structures." *Journal of Vibration and Control* 20 (15): 2352–2365. https://doi.org/10.1177/1077546313486910.

Rathje, E. M., and M. C. Ozbey. 2006. "Site-Specific Validation of Random Vibration Theory-Based Seismic Site Response Analysis." *Journal of Geotechnical and Geoenvironmental Engineering* 132 (7): 911–922. https://doi.org/10.1061/(ASCE)1090-0241(2006)132:7(911).

Rezaeian, S., and A. Der Kiureghian. 2008. "A Stochastic Ground Motion Model with Separable Temporal and Spectral Nonstationarities." *Earthquake Engineering & Structural Dynamics* 37 (13): 1565–1584. https://doi.org/10.1002/eqe.831.

Song, J., and J. Li. 2025. "Stochastic Dynamic Response Analysis Based on Reduced Dimension Probability Evolution Equation Under Additive Gaussian White Noise." *Mechanical Systems and Signal Processing* 233:112747. https://doi.org/10.1016/j.ymssp.2025.112747.

Styron, R., and M. Pagani. 2020. "The GEM Global Active Faults Database." *Earthquake Spectra* 36 (1_suppl): 160–180. https://doi.org/10.1177/8755293020944182.

Tajimi, H. 1960. "A Statistical Method of Determining the Maximum Response of a Building Structure During an Earthquake." *In Proceedings of the 2nd World Conference on Earthquake Engineering*, 781–797. Tokyo, Japan: International Association for Earthquake Engineering.

Tootkaboni, M., and L. Graham-Brady. 2010. "Stochastic Direct Integration Schemes for Dynamic Systems Subjected to Random Excitations." *Probabilistic Engineering Mechanics* 25 (2): 163–171. https://doi.org/10.1016/j.probengmech.2009.10.001.

Vanmarcke, E. H. 1975. "On the Distribution of the First-Passage Time for Normal Stationary Random Processes."

Wang, D., and J. Li. 2011. "Physical Random Function Model of Ground Motions for Engineering Purposes." *Science China Technological Sciences* 54 (1): 175–182. https://doi.org/10.1007/s11431-010-4201-3.

Wang, X., and E. M. Rathje. 2016. "Influence of Peak Factors on Site Amplification from Random Vibration Theory Based Site-Response Analysis." *Bulletin of the Seismological Society of America* 106 (4): 1733–1746. https://doi.org/10.1785/0120150328.

Welch, D. P., T. J. Sullivan, and G. M. Calvi. 2014. "Developing Direct Displacement-Based Procedures for Simplified Loss Assessment in Performance-Based Earthquake Engineering." *Journal of Earthquake Engineering* 18 (2): 290–322. https://doi.org/10.1080/13632469.2013.851046.

Xu, J., and D. C. Feng. 2018. "Seismic Response Analysis of Nonlinear Structures with Uncertain Parameters Under Stochastic Ground Motions." *Soil Dynamics and Earthquake Engineering* 111 (0267-7261): 149–159. https://doi.org/10.1016/j.soildyn.2018.04.023.

Xu, J., Y. Li, J. F. Mao, Z. W. Yu, and S. Tan. 2022. "Dynamic Response and Reliability Analyses of Non-linear Structures Driven by Non-stationary Non-Gaussian Stochastic Ground Motions." *Engineering Structures* 268:114689. https://doi.org/10.1016/j.engstruct.2022.114689.

Zhang, C., J. Xu, Y. Qian, J. Zhang, R. Wang, and B. Wang. 2022. "Seismic Reliability Analysis of Random Parameter Aqueduct Structure Under Random Earthquake." *Soil Dynamics and Earthquake Engineering* 153:107083. https://doi.org/10.1016/j.soildyn.2021.107083.

Zhang, H., X. Xiang, B. Huang, Z. Wu, and H. Chen. 2023. "Static Homotopy Response Analysis of Structure with Random Variables of Arbitrary Distributions by Minimizing Stochastic Residual Error." *Computers & Structures* 288:107153. https://doi.org/10.1016/j.compstruc.2023.107153.

Zhang, H., and Y. G. Zhao. 2022. "Effects of Magnitude and Distance on Spectral and Pseudospectral Acceleration Proximities for High Damping Ratio." *Bulletin of Earthquake Engineering* 20 (8): 3715–3737. https://doi.org/10.1007/s10518-022-01328-9.

Zhang, H., Y. G. Zhao, F. W. Ge, Y. Fang, and T. Ochiai. 2023. "Estimation of Input Energy Spectrum from Pseudo-Velocity Response Spectrum Incorporating the Influences of Magnitude, Distance, and Site Conditions." *Engineering Structures* 274:115165. https://doi.org/10.1016/j.engstruct.2022.115165.

Zhang, R., Y. G. Zhao, and H. Z. Zhang. 2023. "An Efficient Method for Probability Prediction of Peak Ground Acceleration Using Fourier Amplitude Spectral Model." *Journal of Earthquake Engineering* 28 (6): 1495–1511. https://doi.org/10.1080/13632469.2023.2241549.

Zhao, L., Y. Huang, and H. Hu. 2020. "Stochastic Seismic Response of a Slope Based on Large-Scale Shaking-Table Tests." *Engineering Geology* 277:105782. https://doi.org/10.1016/j.enggeo.2020.105782.